Self-constraining of low-energy rivers explains low channel mobility and tortuous planforms

Candel, Jasper H.J.; Makaske, Bart; Kijm, Niels; Kleinhans, Maarten G.; Storms, Joep E.A.; Wallinga, Jakob

DOI
10.1002/dep2.112

Publication date
2020

Document Version
Final published version

Published in
Depositional Record

Received: 6 September 2019 | Revised: 19 March 2020 | Accepted: 24 March 2020

DOI: 10.1002/dep2.112

ORIGINAL RESEARCH ARTICLE

The Depositional Record Open Access
A journal of the International Association of Sedimentologists
WILEY

Self-constraining of low-energy rivers explains low channel mobility and tortuous planforms

Jasper H. J. Candel[1] | **Bart Makaske**[1] | **Niels Kijm**[1] | **Maarten G. Kleinhans**[2] | **Joep E. A. Storms**[3] | **Jakob Wallinga**[1]

[1]Soil Geography and Landscape Group, Wageningen University and Research, Wageningen, The Netherlands

[2]Department of Physical Geography, Faculty of Geosciences, Utrecht University, Utrecht, The Netherlands

[3]Faculty of Civil Engineering and Geosciences, Delft University of Technology, Delft, The Netherlands

Correspondence
Jasper H. J. Candel, Wageningen University & Research, Wageningen, The Netherlands.
Email: jasper.candel@wur.nl.

Funding information
Nederlandse Organisatie voor Wetenschappelijk Onderzoek, Grant/Award Number: P12-14; NWO, Grant/Award Number: 016, 140, 316 and 13710

Abstract

Meandering rivers are abundant on Earth, from the largest rivers to the smallest tributaries. The classical view of meandering rivers is a sinuous planform with rounded bends, which grow and migrate until they are cut-off. However, many low-energy meandering rivers have planforms that are much more complex than this classical view due to the heterogeneity of their alluvium, and show relatively limited channel migration. Based on a detailed palaeogeographic study of the Dommel River in The Netherlands, it is inferred that low-energy meandering rivers may develop tortuous planforms with sharp bends, owing to self-formed deposits that increasingly constrain the channel mobility. This mechanism is corroborated by data from 47 meandering river reaches of varied scale from around the world, which show that erosion-resistant floodplain deposits are preserved in the river banks when the river energy is below a critical threshold. The term 'self-constraining' is proposed for low-energy rivers where an increase in bank stability over time results in progressive tortuous planforms and reduced mobility. A conceptual model, based on the dataset, shows that the increase in bank stability over time also increases the energy required to break out of the tendency to self-constrain. Self-constraining thereby enhances the resilience of the system to bank erosion, while an unexpected increase in bank erosion may occur if river energy exceeds the critical threshold. This study provides a novel explanation for the evolution of low-energy river planforms and dynamics, and provides new insights on their responses to climate changes.

KEYWORDS

fluvial morphology, heterogeneous floodplain architecture, Holocene, river channel planform

1 | INTRODUCTION

Meander bend formation has been extensively studied by earth scientists, hydrologists and engineers (Friedkin, 1945; Leopold and Wolman, 1957; Ikeda and Parker, 1989; Stølum, 1996; Seminara, 2006; Camporeale *et al.*, 2007; Gibling and Davies, 2012; Lazarus and Constantine, 2013). Widely accepted is the concept that river bends form due to instability between the flow and bed, amplified by bend flow (Struiksma *et al.*, 1985; Ikeda and Parker, 1989; Seminara, 2006). This

classical model forms the basis of both physical and numerical river meander migration models, which produce simulations of freely meandering patterns with rounded bends and continuous lateral migration (Crosato, 2009; Kleinhans, 2010; Motta *et al.*, 2012b). However, natural meandering rivers have a wide range of planform complexities (Figure 1), and not all rivers with sinuous planforms show lateral migration (Hickin and Nanson, 1984; Güneralp and Rhoads, 2011; Kleinhans and Van den Berg, 2011; Vermeulen *et al.*, 2014; Candel *et al.*, 2017).

The term 'tortuosity' was introduced by Schumm (1963), and used to refer to rivers with complex planforms consisting of unusually sharp bends with variable size and abrupt, irregular changes in channel direction, lacking the typical smoothness of ideal meander curves (Figure 1A through D). This definition of tortuosity is adopted here, and is radically different from the use of tortuosity as a synonym for sinuosity by some others (Frascati and Lanzoni, 2009). Sharp bends are commonly defined as $\frac{R_{curv}}{w} < 2.0$ (R_{curv} = bend curvature, w = channel width), and form when outer banks are relatively erosion-resistant compared to the river stream power (Leeder and Bridges, 1975; Ferguson *et al.*, 2003; Makaske and Weerts, 2005). Field measurements by Schumm (1963) showed that greater river tortuosity relates to larger silt-plus-clay (SC) fractions of river banks. Subsequent research indicated that large SC-fractions are typically found in low-energy meandering rivers (Nanson and Croke, 1992). More recently, numerical modelling studies showed that tortuous planforms develop when heterogeneous floodplains are included in the simulations, consisting of depositional units with different resistances to erosion (Camporeale *et al.*, 2005; Güneralp and

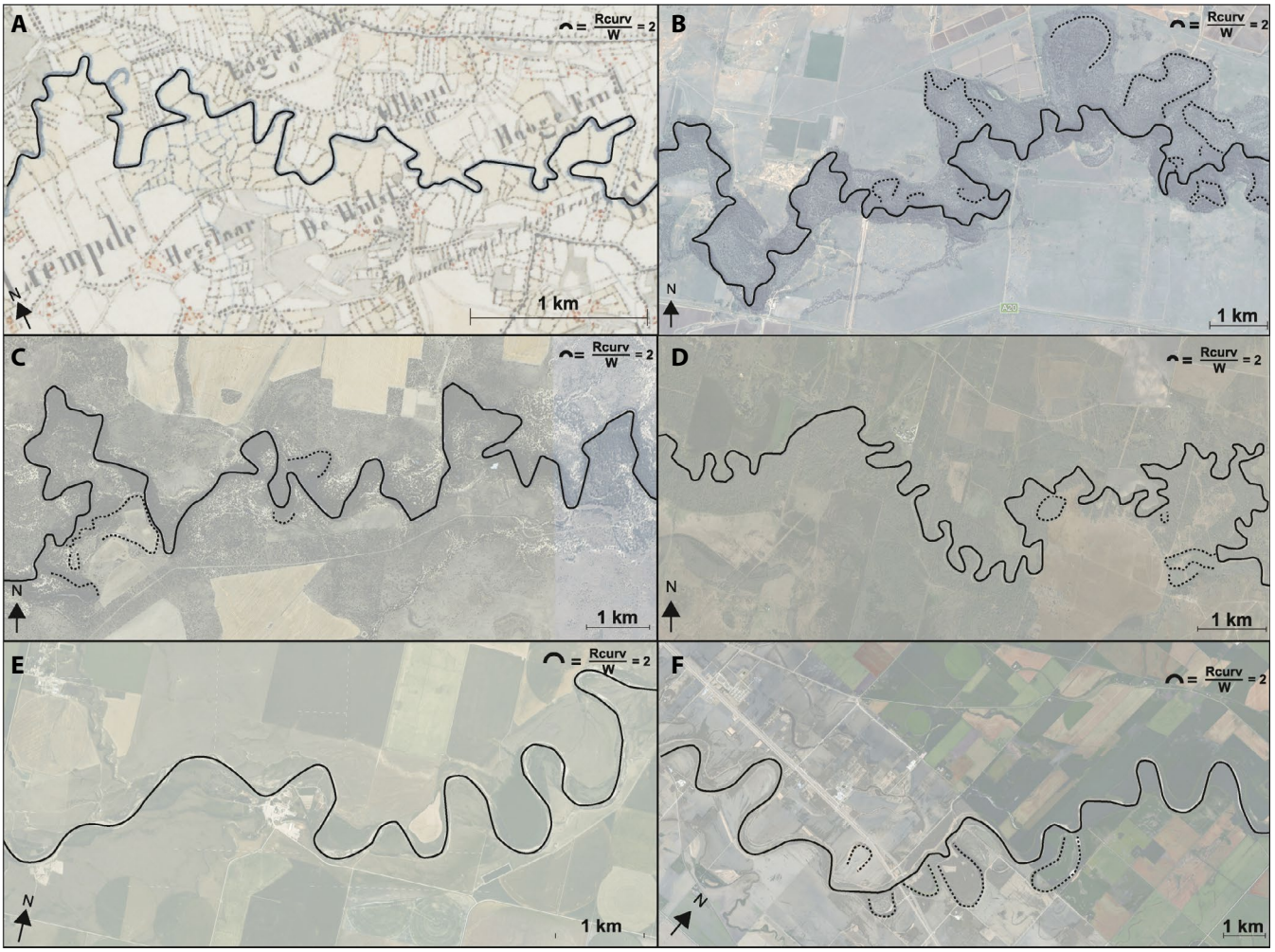

FIGURE 1 River planforms throughout the world, A through D showing tortuous meandering planforms, and E and F showing relatively classical meandering planforms, derived from Google Earth satellite imagery (2018) for B through F. All planforms are scaled to five predicted meander amplitudes (Carlston, 1965). (A) Dommel River in The Netherlands before the channelization, the planform was derived from the Topographical Military Map (TMK) dating from 1837 CE (Van der Linden, 1973) (51°34′12.3″N 5°24′43.6″E). (B) Murrumbidgee River in Australia (34°26′23.6″S 145°29′43.5″E). (C) Barwon River in Australia (30°00′00.0″S 147°58′00.0″E). (D) San Antonio River in USA (28°32′28.6″N 97°04′25.7″W). (E) Waterton River in Canada (49°26′22.87″N 113°27′33.36″W). (F) Assiniboine River in Canada (49°58′20.82″N 98°7′20.61″W)

Rhoads, 2011; Motta *et al.*, 2012a; Bogoni *et al.*, 2017). These authors stress that floodplain heterogeneity is an important control on planform complexity in (simulated) meandering rivers. Additionally, Hudson and Kesel (2000), who compared sections of different floodplain heterogeneity in the Mississippi River, found that average lateral migration rates are lowest where floodplain heterogeneity is highest. The authors explain this by greater presence of cohesive (silty and clayey) and organic-rich deposits (e.g. clay plugs), which can be 10–20 times more erosion-resistant than non-cohesive (sandy) units (Hjulstrom, 1935).

Although relationships have been described in previous studies of lateral migration rates, bend curvature and floodplain sediment composition, a proper conceptual model on low-energy river planform development is still lacking. Based on earlier publications, it is hypothesized that low-energy meandering rivers in heterogeneous floodplains predominantly erode the easily erodible, non-cohesive depositional units (Turnbull *et al.*, 1966; Hickin and Nanson, 1984), while they continuously form both easily erodible (e.g. point-bar) and relatively erosion-resistant (e.g. residual channel-fill) depositional units (Smith *et al.*, 2009; Bogoni *et al.*, 2017). This mechanism may explain why low-energy meandering rivers tend to have tortuous planforms with low channel mobility.

The main aims of this paper are: (a) to test the hypothesis of a relationship between inhibited lateral channel mobility, planform tortuosity and the evolution of floodplain sediment composition, and (b) to define the parameter space of river energy and bank erosion-resistance at which this conceptual model applies. Toward the first aim, the long-term evolution of the low-energy meandering Dommel River (The Netherlands) is reconstructed in detail. The second aim is addressed by analysing a large dataset of meandering rivers with data available on stream power, river energy (i.e. stream power), bed material and SC-fractions of the banks.

2 | MATERIALS AND METHODS

2.1 | Study area

The Holocene planform evolution and floodplain stratigraphy of the Dommel River (Figure 2), a low-energy meandering sand-bed river with a tortuous planform, was studied. This investigation combined coring, ground-penetrating radar (GPR) and geochronological analysis around four oxbow bend complexes. The Dommel River's source is located at the Kempen Plateau in Belgium, +77 m NAP (Dutch Ordnance Datum, ≈sea level), and drains into the much larger River Meuse at + 2 m NAP (Figure 2). It has a length of 120 km of which 85 km is located in The Netherlands. The catchment size is *ca* 677 km^2. The river has an annual average discharge of 14 m^3/s and a mean annual flood discharge of 22.3 m^3/s at its downstream end.

The Dommel River was a braiding river during the Pleniglacial with abundant sediment availability, and low average discharges and transport capacity (Vandenberghe and Bohncke, 1985; Vandenberghe and Van Huissteden, 1988). The cold and dry climate and absence of vegetation during the Pleniglacial resulted in large-scale deposition of coversand 0.5–2 m thick in the study area, which currently overlies all older deposits outside the valley (Van der Hammen, 1971; Vandenberghe and Bohncke, 1985). Locally, the coversands are very fine-grained and would more properly be called loess and sandy loess, referred to as 'Brabant loam' or the Liempde Member of the Boxtel Formation (Vink, 1949; Schokker, 2003). The climate changed to warmer and wetter conditions at the Pleniglacial to Late Glacial transition, and vegetation re-established. Consequently, the sediment availability decreased and the river discharge increased resulting in a relatively large, incising meandering river (Vandenberghe and Bohncke, 1985; Vandenberghe and Van Huissteden, 1988; Vandenberghe, 1995). The result of the Late Glacial meandering phase is a well-expressed bluff along the edge of the valley (Figure 2C through F).

This research focusses on planform and morphological development of the Dommel River during the relatively warm and wet Holocene. Historic maps show that around 1890 calibrated calendar age (CE) the river had a tortuous planform that was hardly affected by humans, except for some local modifications related to weirs and watermills (Waterschap De Dommel, 1941; Figure 1A). After 1890 CE, many river bends and bend complexes were cut-off to promote rapid drainage of the catchment (Waterschap De Dommel, 1941). Palynological data for the Dommel Valley (Janssen, 1972; Van Leeuwaarden, 1982) are available for the entire Holocene and indicate relatively small-scale human cultivation on the higher grounds around 500 BCE, while these areas were increasingly being used for agriculture after 1000 CE with the cultivation of buckwheat, rye and pine. The valley was used largely as pasture. Currently, the land use around the Dommel River is forest and agriculture (cattle and arable farming).

There is little morphological evidence of active channel migration prior to river normalization; some oxbow complexes are present, but no scroll-bar forms are observed (Figure 2D through F). The historical map of 1837 CE shows how these bend complexes were still part of the main river (Figure 1A). Figure 2 shows three selected research sites in the Dommel River, which were selected based on the presence of oxbow lakes. These oxbow lakes are well-preserved in the landscape and consist of sharp bend complexes, similar to Dommel River bends that are still connected to the river (Van Alphen *et al.*, 1984).

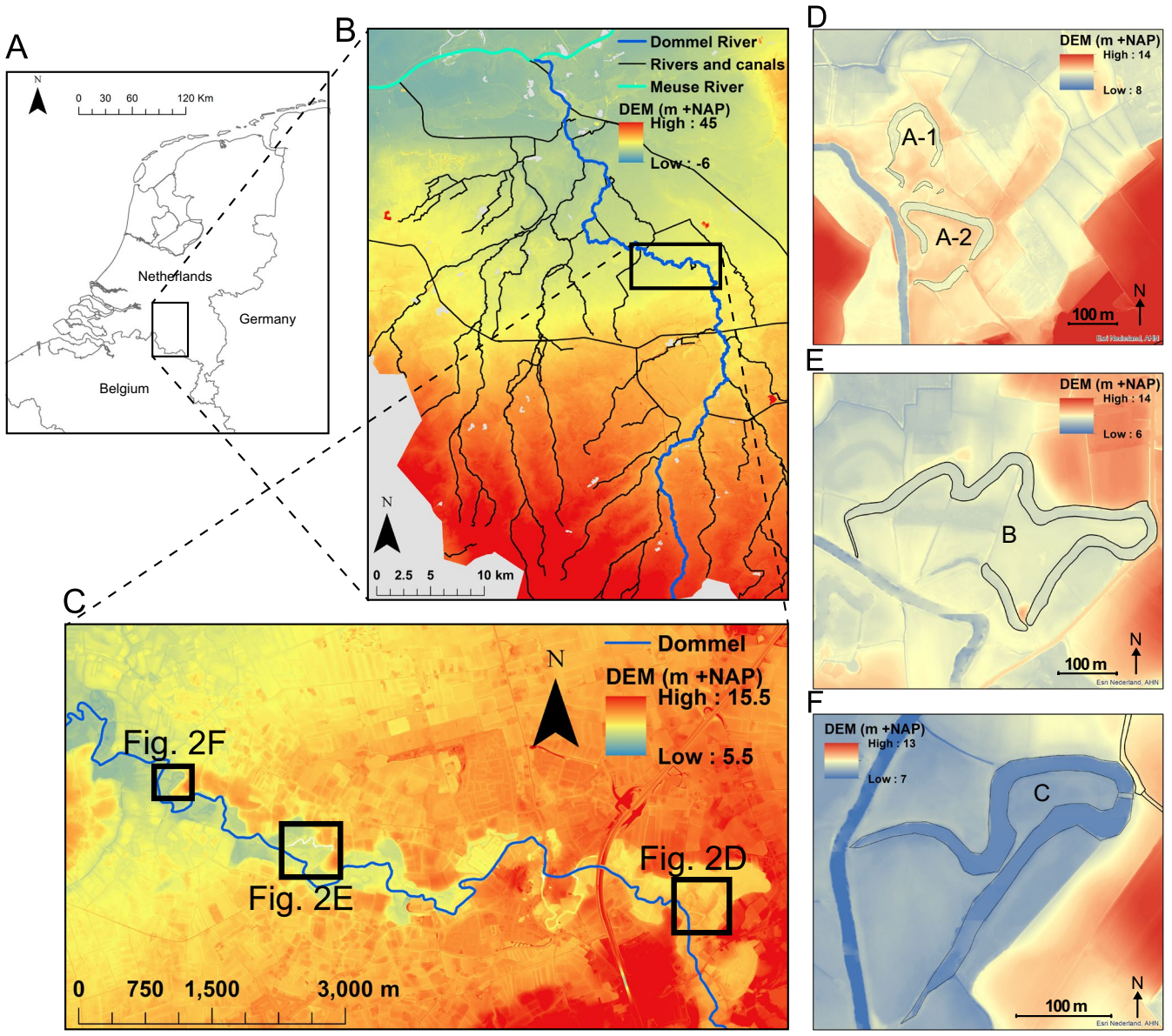

FIGURE 2 Maps of the Dommel River. (A) Map showing the location of the Dommel River in The Netherlands. (B) A digital elevation map (DEM, Actueel Hoogtebestand Nederland, 0.5 x 0.5 m grid) (Van Heerd and Van't Zand, 1999) of the Dutch section of the Dommel river. All study sites are indicated. (C) DEM of the three study locations A,B and C, showing the oxbow bend complexes (D through F)

2.2 | Ground-penetrating radar

Ground-penetrating radar was used to select suitable coring locations based on stratigraphic differences, and to support the interpretation of the lithological borehole cross-sections. The GPR measurements were conducted with a pulseEKKO PRO 250 Hz with a SmartTow configuration. The GPR was used in different directions relative to the bend complexes (Figure 3). In a sandy subsurface, lateral accretion surfaces and palaeochannels can usually be detected with a GPR (e.g. Figure 4). Loamy and peaty subsurfaces strongly attenuate the GPR signature (Neal, 2004), resulting in poor GPR images and no information on subsurface structure. For this study area, the electromagnetic-wave velocity was determined to be 0.052 m/ns, derived by using isolated reflector points (Van Heteren *et al.*, 1998; Neal, 2004) in the EKKO_Project™ software, and by comparing depths of recognizable layers with the coring data.

2.3 | Coring and Lithology

Hand corings were performed along the inside and outside of the river bend complexes (Figure 3). The surface elevation of each coring site was determined using a GPS combined with the digital elevation map (DEM) (0.5 × 0.5 m grid; Van Heerd and Van't Zand, 1999). A gouge auger (Ø 3 cm) was used when the subsurface consisted of peat or

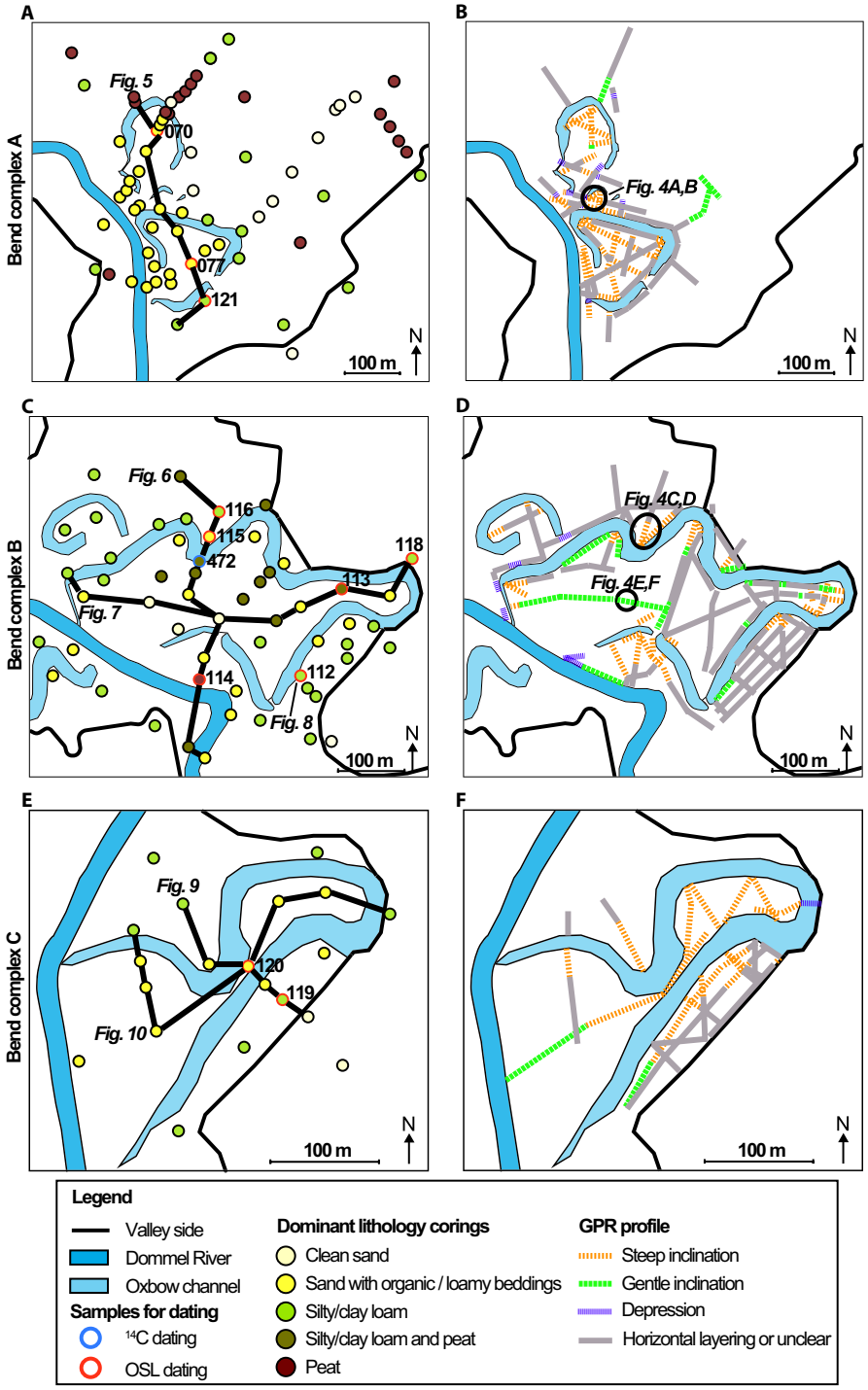

FIGURE 3 Maps of the study locations. (A, C, E) Simplified maps showing the coring, dating and transect locations. The colour infill of the coring locations indicate the main lithology that was found. The lines indicate the transects shown in Figures 5 through 10. The numbers refer to the last three digits of the OSL and ^{14}C sample codes, and indicate the sampling locations (Table 1). (B, D, F) Simplified maps showing the GPR profile locations; colours denote the observed structures. Some examples are given in Figure 4

water-saturated loam, an Edelman auger for unsaturated loam or sand and a Van der Staay suction corer (Van de Meene *et al.*, 1979) for saturated sand. In total, 130 corings were performed to a maximum depth of 5.9 m. Lithology of sediment cores was described in 10 cm thick intervals, using the USDA nomenclature (Berendsen and Stouthamer, 2001). The sediment grain size (D_{50}) of non-organic, sandy samples was visually checked in the field by comparison with a sand ruler. In addition, the plant macro-remains, any visible bedding, colour and presence of gravel were described.

The lithological data are presented in five lithological cross-sections (Figures 5A through 10A). For each of the sections, a lithogenetic interpretation was inferred from the lithological properties, facies geometries and GPR data (Figures 5B through 10B). In Section 3.1, maps are presented of the locations of erosion-resistant layers, defined as peaty or loamy layers with a minimum thickness of 0.5 m.

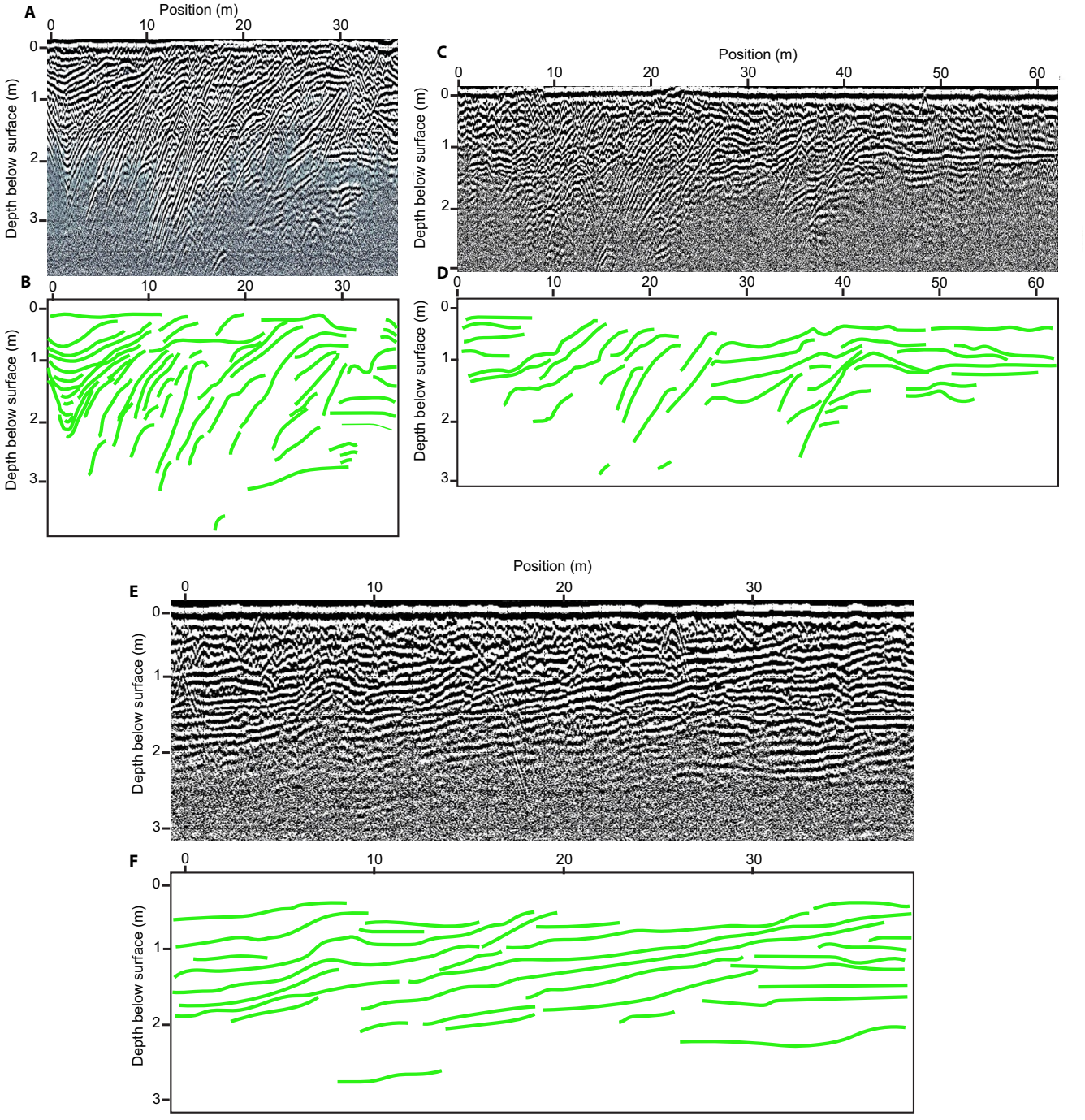

FIGURE 4 GPR transect examples. Locations are shown in Figure 3. (A, C, E) Plain GPR data. (B, D, F) Interpreted subsurface strata

2.4 | Optically stimulated luminescence dating

Eleven samples for quartz optically stimulated luminescence (OSL) dating were taken to determine the age of erosion-resistant layers and point-bar deposits (Figure 3). Samples were collected in a PVC tube (Ø 4 cm, 25 cm length) with a Van der Staay suction corer (Van de Meene *et al.*, 1979; Wallinga and Van der Staay, 1999), allowing collection of non-light-exposed sand in the middle of the tube. The OSL age was determined at the Netherlands Centre for Luminescence dating, Wageningen University. Approximately 150 g of sediment, from the light-exposed outer ends of the tubes, was used for the dose rate analysis, and the remaining sediment was prepared for equivalent dose estimation.

For dose rate estimation, samples were dried and ashed to remove water and organics and determine their weight fractions. Samples were ground and mixed with wax and moulded in a puck to ensure radon retention and provide a fixed geometry for measurement. Radionuclide concentrations were determined using high-resolution gamma-ray spectroscopy, and converted into infinite matrix dose rates

TABLE 1 OSL and ^{14}C dating results of the Dommel River. The sample codes correspond to the codes given in Figure 3

Sample Code	Lat, Lon (RD)	Lithology	Surface elevation (m + NAP)	Sample depth interval (m)	^{14}C age (BP)	Palaeodose (Gy)	Dose rate (Gy/ka)	Age (ka)
NCL2117**112**	157825 397437	Loam	8.63	0.90–1.20		4.1 ± 0.2	1.65 ± 0.09	2.5 ± 0.2
NCL2117**113**	157887 397566	Sand	8.58	2.20–2.50		1.9 ± 0.2	0.85 ± 0.04	2.2 ± 0.3
NCL2117**114**	157675 397432	Sand	8.81	2.55–2.85		1.0 ± 0.2	0.74 ± 0.04	1.3 ± 0.3
NCL2117**115**	157690 397643	Sand	8.67	1.60–1.90		0.5 ± 0.1	0.70 ± 0.03	0.7 ± 0.1
NCL2117**116**	157705 397681	Sand	8.57	2.15–2.35		9.1 ± 1.2	1.07 ± 0.06	8.5 ± 1.2
NCL2117**118**	157993 397610	Clay loam	9.32	1.50		36.7 ± 2.9	2.51 ± 0.12	14.6 ± 1.4
NCL2117**119**	156242 398294	Clay loam	7.81	1.50–1.80		3.0 ± 0.1	1.05 ± 0.06	2.8 ± 0.2
NCL2117**120**	156210 398324	Sand	7.99	1.95–2.25		3.7 ± 0.2	0.78 ± 0.04	4.7 ± 0.4
NCL2117**121**	162125 396686	Clay	10.49	1.50–1.85		8.9 ± 0.6	1.15 ± 0.08	7.8 ± 0.8
NCL2116**070**	162038 397000	Sand	10.37	2.20–2.50		1.7 ± 0.2	0.72 ± 0.02	2.3 ± 0.3
NCL2116**077**	162104 396718	Sand	10.51	2.25–2.50		0.4 ± 0.1	0.68 ± 0.03	0.6 ± 0.1
GrM10**472**	157676 397606	Peat	8.62	2.9–3.1	8,610 ± 20			9.6 ± 0.2

(Guérin *et al.*, 2011). Attenuation by water and organics (Aitken, 1998) were taken into account, based on present water and organic content. Grain size attenuation was taken into account for beta dose rate estimation (Mejdahl, 1979). A contribution of cosmic dose rates was included following Prescott and Hutton (1994), and assuming immediate burial to present depth. A minor contribution from internal alpha irradiation inside the quartz grains (Vandenberghe *et al.*, 2008) was also included.

For equivalent dose estimation sand-sized grains of quartz (180–212 μm) were obtained through sieving and treatment with HCl, H_2O_2 and HF. For each sample, small aliquots (2 mm diameter, about 75 grains) were prepared on stainless-steel disks sprayed with silicon oil. Measurements were performed on a Risø TL/OSL DA20 reader (Bøtter-Jensen *et al.*, 2003), using the single-aliquot regenerative dose (SAR) protocol (Wintle and Murray, 2006). A relatively low preheat of 200°C for 10s and 10s 'cutheat' of 180°C were used, to prevent thermal transfer effects. Early-background subtraction was used to maximize the contribution from the quartz fast-OSL component (Cunningham and Wallinga, 2010). Around 40 aliquots were measured per sample. The Central Age Model (Galbraith *et al.*, 1999) was used to determine overdispersion for all samples. This model was also used to determine the palaeodose (best-estimate of the burial dose) for the sample of aeolian sediment taken from the valley side (NCL-2117118; Table 1). The overdispersion not related to heterogeneous bleaching (σ_b) was estimated to be 17 ± 7% (Cunningham *et al.*, 2011), and used as sigma$_b$ input for the bootstrapped version of the Minimum Age Model (Galbraith *et al.*, 1999; Cunningham and Wallinga, 2012), which was used to determine palaeodoses from scattered equivalent dose distributions for all fluvial samples. Burial ages were determined by dividing the palaeodose by the dose rate, taking all uncertainties in both into account. Following conventions, results are reported in ka relative to the year of sampling (2017 CE) with 1-sigma errors (Table 1).

2.5 | ^{14}C Dating

A single sample for ^{14}C dating was taken from a residual channel-fill using a gouge auger (Ø 6 cm; Figure 3C; sample 472). Macro-remains from terrestrial species (e.g. sedge) were selected in the laboratory using a light microscope. Samples were stored in diluted HCl (4%) at 5°C. The ^{14}C age was determined by Accelerator Mass Spectrometry at the Centre for Isotope Research (Groningen University). For calibration, the IntCal13 curve was used in the OxCal4.2.4 software (Bronk Ramsey, 2009; Reimer *et al.*, 2013). Following conventions, uncalibrated radiocarbon age (BP) and CE are reported.

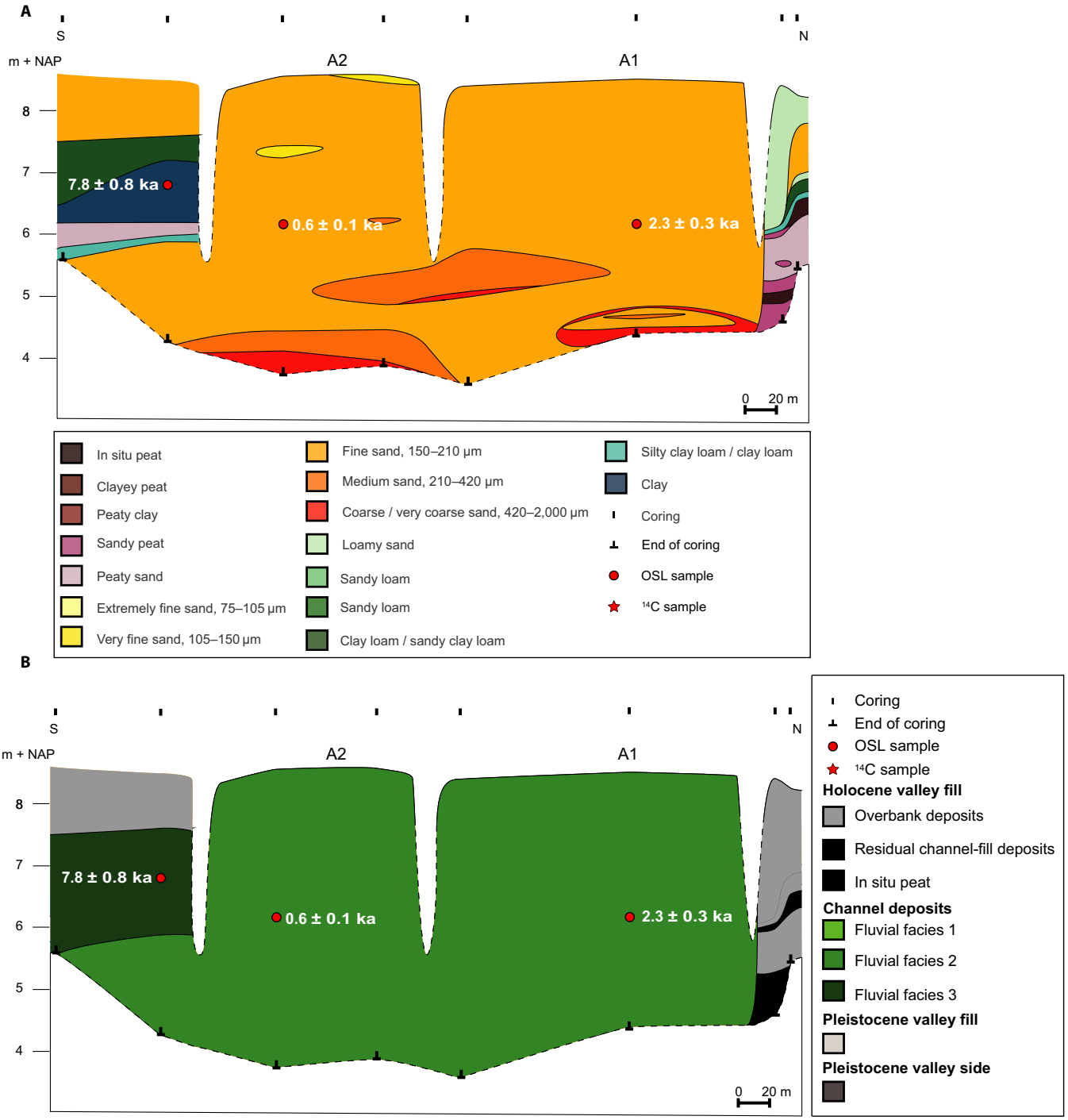

FIGURE 5 Cross-sections of the valley-fill (location in Figure 3A) including the OSL sample locations. (A) Lithological cross-section. (B) Lithogenetic cross-section. Location of the bend complex A-1 and A-2 are indicated (see Figure 2D)

2.6 | Comparison to other meandering rivers

The dataset of Kleinhans and Van den Berg (2011) was used as an analytical starting point, because similar data and selection criteria were required. The data contained in this dataset are mean annual flood discharge, bankfull discharge, median bed grainsize and valley slope. In addition, the average silt-plus-clay fraction of the river banks and tortuosity of the channel planform were determined (see below). All studied meandering rivers are alluvial rivers that have no sign of strong modification by humans, no engineering in the river, a perennial flow regime, and an effective channel-forming discharge (Q_{eff}) >10 m^3/s (mean annual flood, and when not available the bankfull discharge was taken, see argumentation of choice given by

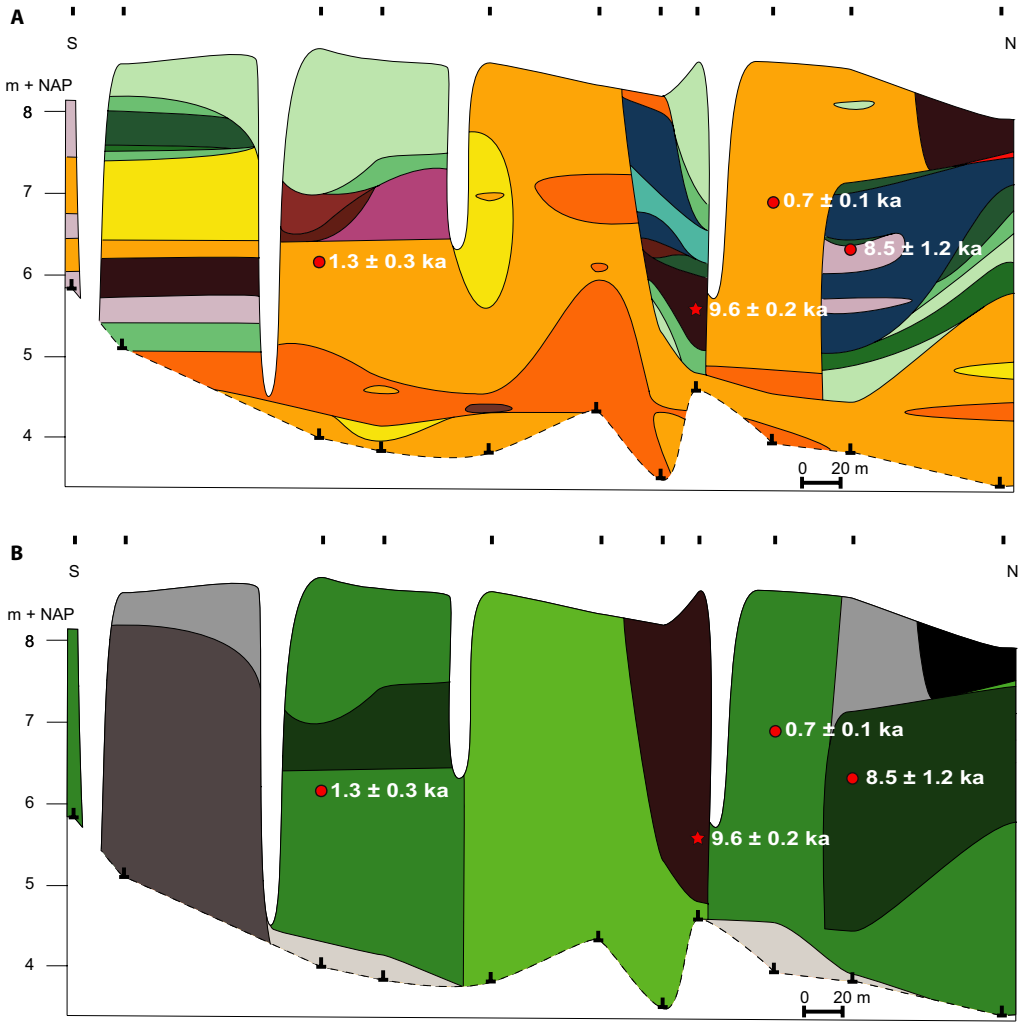

FIGURE 6 Cross-sections of the valley-fill (location in Figure 3C) including the OSL and ^{14}C sample locations. (A) Lithological cross-section. (B) Lithogenetic cross-section. Legend indicated in Figure 5

Kleinhans and Van den Berg, 2011). All rivers are laterally connected with their floodplain, and are not strongly incising or aggrading. The dataset of Kleinhans and Van den Berg (2011) sometimes included multiple reaches of the same river for which different values of Q_{eff} or valley slope (S_v) were found.

From this dataset, a subset of meandering river reaches was selected for which published information on average SC-fractions of the river bank was available in the literature. Estimates on average SC-fractions of the fluvial depositional units are taken as a measure of the erosion-resistance of the floodplain units following Hjulstrom (1935), Schumm (1963) and Julian and Torres (2006), as this is the only suitable parameter that is abundantly available and was previously linked to tortuosity (Schumm, 1963). These river banks represent either depositional units of the river or the valley side. A high or low average silt-plus-clay fraction of the river banks suggests they consist of relatively erosion-resistant or easily erodible depositional units, respectively. Data were not included if SC-fractions were only qualitatively described. Where ranges of SC-fractions were reported, the middle of the range was used. Sampling methods and texture analysis varied between studies that reported average SC-fractions; see cited sources in the Supplementary Data for details. Generally, multiple samples were taken of both river banks near the gauging stations, often at several depths from the exposed river bank. Samples were in most cases analysed in the laboratory using the sieving and pipette method.

Kleinhans and Van den Berg (2011) showed that the potential specific stream power (ω_{pot}) is a suitable measure for river energy to explain the degree of meandering. The potential specific stream power was calculated by applying the relationship presented by Kleinhans and Van den Berg (2011):

$$\omega_{pot} = \frac{\rho g \sqrt{Q_{eff}} S_v}{\varepsilon} \quad (1)$$

where ω_{pv} is the potential specific stream power (W/m^2), ρ the water density (kg/m^3), g the gravitational acceleration (m/s^2),

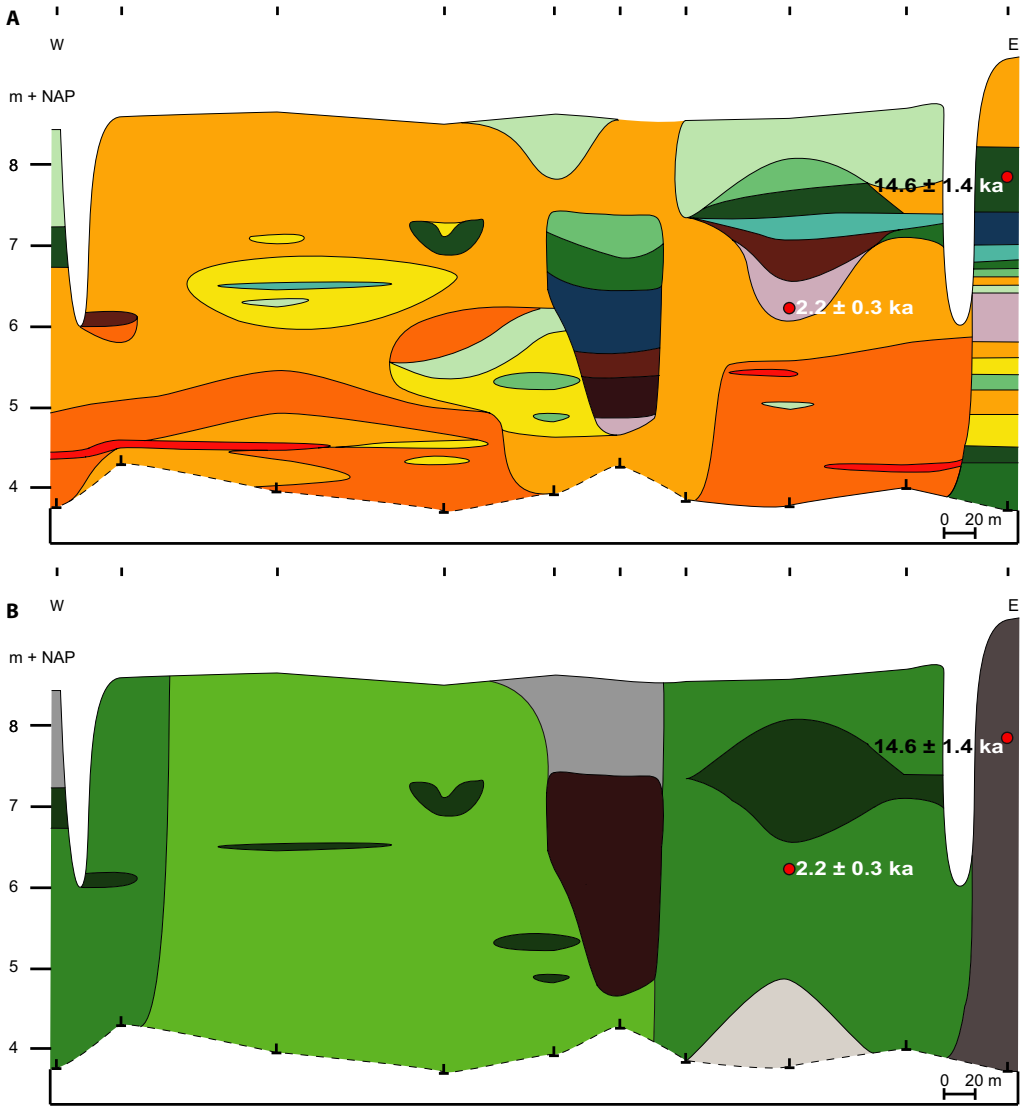

FIGURE 7 Cross-sections of the valley-fill (location in Figure 3C) including the OSL and ^{14}C sample locations. (A) Lithological cross-section. (B) Lithogenetic cross-section. Legend indicated in Figure 5

and coefficient $\varepsilon = 4.7\sqrt{sm^{-1}}$ for sand-bed rivers and $\varepsilon = 3.0\sqrt{sm^{-1}}$ for gravel-bed rivers (Van den Berg, 1995). A large advantage of the potential specific stream power as a measure for river energy is that it relies on parameters that are independent of the actual channel planform, and hence can be used to explain the planform tortuosity of a river (Van den Berg, 1995).

There is thought to be no widely accepted metric to quantify planform tortuosity (ignoring the metric proposed that is based on channel length divided by valley length, and thus reflects sinuosity rather than tortuosity). Here a new metric is proposed, based on the fraction of bends that are 'sharp' with a $\frac{R_{curv}}{w} < 2.0$ (R_{curv} = bend curvature, w = channel width). To estimate this metric, bend curvature of the channel centreline and average channel width of each bend were determined using satellite imagery from Google Earth for 20 consecutive meander bends in the river reaches contained in the Kleinhans and Van den Berg (2011) dataset. Including more bends in this measure would result in sharp bend measurements that are taken too far from the measurements of the other parameters.

The resulting dataset was supplemented with information from the Dommel River (this study), and the Overijsselse Vecht (recently studied by Candel *et al.*, 2018). Finally, data for two Late-Glacial rivers were included (Dommel and Niers), based on channel patterns recognizable from DEMs or satellite imagery, and published information on average SC-fraction of the surrounding depositional units (see Supplementary Data for references). The Late-Glacial Dommel River had a bankfull discharge of a factor 12–15 higher than the current Dommel River (Vandenberghe, 2001). Valley slope was estimated using the depths of Late-Glacial deposits from DINOloket, a national geological borehole database (TNO, 2015). Data for the Late-Glacial Niers River were derived from Kasse *et al.* (2005). Planform tortuosity of

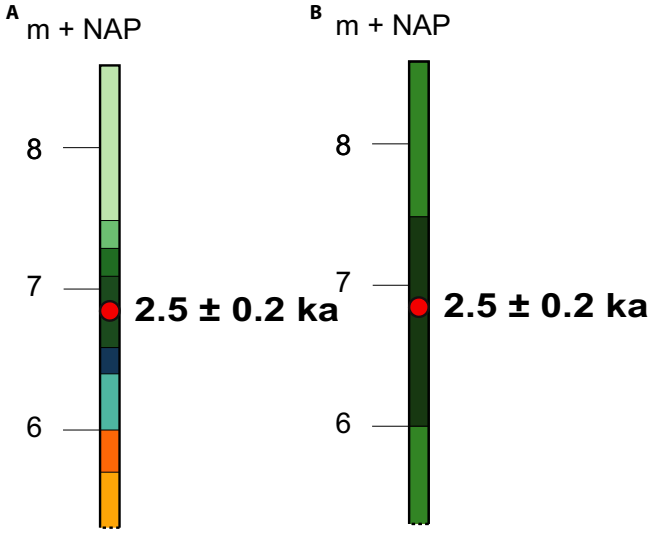

FIGURE 8 Borehole of the valley-fill (location in Figure 3C) including the OSL location. (A) Lithological sequence. (B) Lithogenetic sequence. Legend indicated in Figure 5

Late-Glacial rivers was measured from visible palaeochannels on DEMs or satellite imagery or from the valley side bluffs, divided by the estimated width of the Late-Glacial systems known from Late-Glacial oxbow channels.

3 | RESULTS

3.1 | Lithogenetic units

Lithogenetic units were identified within the Holocene Dommel River valley-fill based on lithology, planform, facies architecture (GPR) and interpreted genesis. In general, the Holocene valley-fill can be distinguished from bordering Pleistocene valley side deposits and underlying Pleistocene valley-fill deposits by the presence of organic matter (OM), for example, recognizable plant remains, and dark colours (Bisschops, 1973; Berendsen and Stouthamer, 2000; Huisink, 2000).

The Pleistocene valley-fill deposits consist of very fine to medium fine sand (105–420 μm), with a light, bright colour, sometimes with small fining upward sequences several decimetres thick. Thick beds (several decimetres) of loam or OM are absent (Bisschops, 1973; Schokker and Koster, 2004), but thin gravel beds up to a decimetre thick can be found within the unit. The top of the Pleistocene valley-fill is usually found *ca* 4–5 m below the surface (Bisschops, 1973).

The Pleistocene valley side can clearly be distinguished from the valley-fill due to its higher surface position. The valley side consists of the sedimentological units coversand (Bisschops, 1973), which partly consists of 'Brabant loam' (Vink, 1949; Schokker, 2003), and fluvioperiglacial deposits (Bisschops, 1973). Locally, strongly consolidated, in situ peat can be found within the unit. The texture ranges from very fine sand to medium fine sand (105–420 μm), and loamy sand to clay loam. The colours are light grey, brown and yellow. Beds of OM are mostly absent, except for sporadically occurring laminae several millimetres thick.

The lithogenetic units that form the Holocene valley-fill are elaborated on here.

Overbank deposits consist of very fine sand to fine sand (median grain size 105–210 μm), peaty sand and loamy sand to clay loam. The colour of the unit is usually light grey to dark brown. The OM content is low (<1%) when not peaty. Sometimes small fractions of reworked plant remains or loam are present, which occur in layers of several millimetres to several centimetres in thickness. The unit mostly overlies the other units, but can be found within the unit in situ peat as well. The unit is usually found near a channel or channel-fill, and has a thickness of 1–2 m, but becomes thinner further away from the channel or channel-fill. The unit can be recognized by its horizontal layering in the GPR profiles when the GPR results are of sufficient quality (Figure 3).

Residual channel-fill deposits range in texture from loamy sand to clay loam, peaty sand and clayey peat. In situ peat can be present near the base of the unit. The colour of the unit is mostly dark brown, grey, green or blue. The unit is generally humic (OM content 2%–4%) or very humic (OM content 4%–8%). The unit is structureless when consisting of peat, or else consists of layers of OM, sand or loam with thicknesses of several millimetres to several centimetres. The degree of consolidation increases with depth when overlain by sediments, and the unit was difficult to core below *ca* 2 m depth. The unit has a relatively low width/thickness ratio, a thickness of 2.5–4 m, and is located on top of and alongside channel deposits. The unit strongly reflects the GPR signal, but the unit base can be recognized in the GPR profile as a concave structure (i.e. depression, Figure 3). When the GPR profile quality allows, the horizontal or concave layering can be recognized within the unit (e.g. Figure 4A,B).

Channel deposits were split into three different fluvial facies, in order to distinguish different types of channel deposits. Fluvial facies 1 consists of moderately well-sorted clastic sediments varying in texture from very fine sand to coarse sand (median grain size 105–600 μm). The colour of the unit is light brown to dark grey. A fining upward sequence is often present with medium fine to coarse sand at the bottom of the unit (channel lag) containing up to 15% gravel, followed by very fine sand, loamy sand or sandy loam at the top. The colour of Fluvial facies 1 is light grey or brown. Organic and loamy beds are mostly absent. The unit has a thickness of 4–5 m and reaches the present surface, although the unit is generally not recognizable from the topography. Except for its near surface location, the unit is relatively difficult to distinguish from the Pleistocene valley-fill. Gently inclined strata (1°–3°) can be visible in the GPR profile (Figures 3 and 4E,F). Fluvial

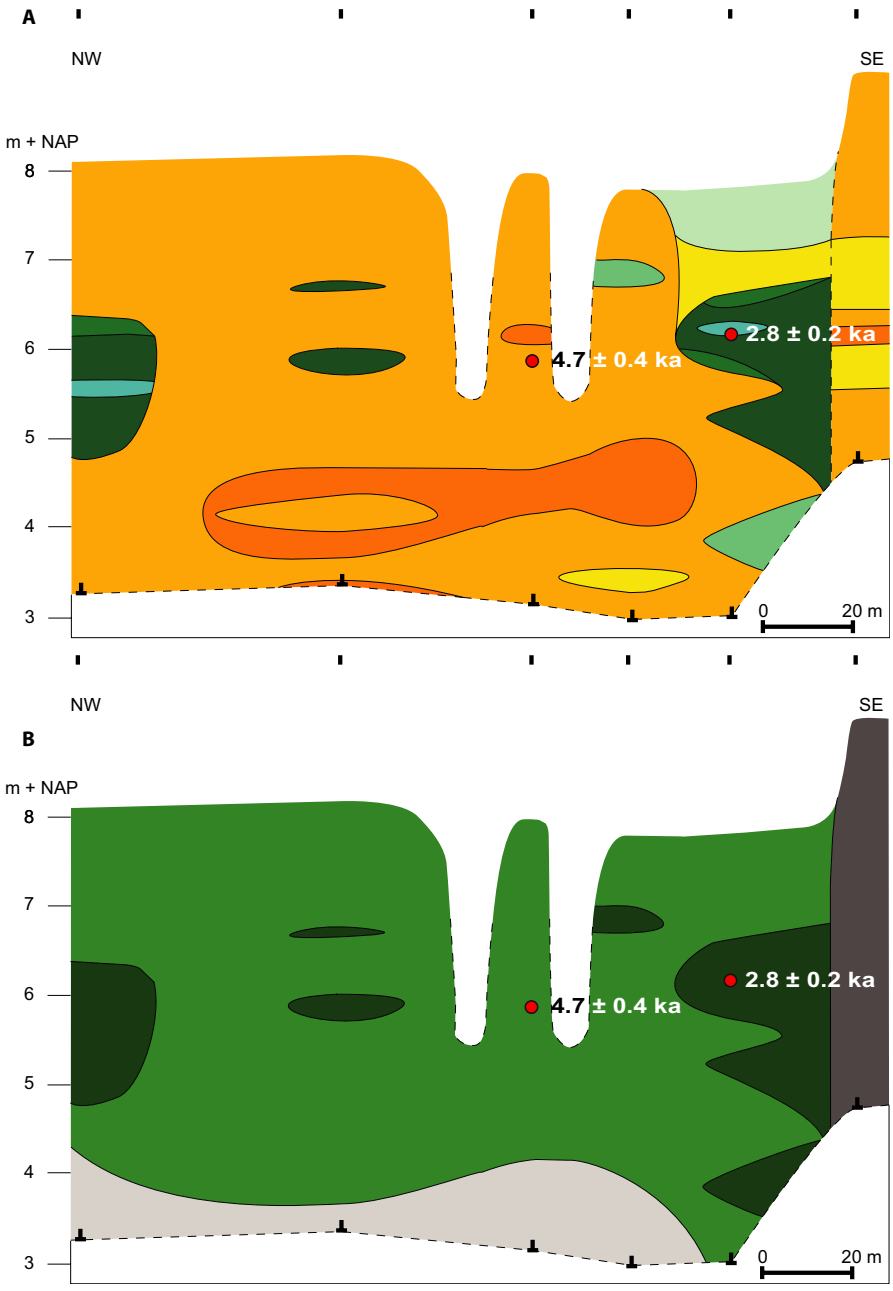

FIGURE 9 Cross-sections of the valley-fill (location in Figure 3E) including the OSL sample locations. (A) Lithological cross-section. (B) Lithogenetic cross-section. Legend indicated in Figure 5

facies 2 is similar to Fluvial facies 1 based on texture, geometry, extent and the presence of a fining upward textural trend. However, the colour of Fluvial facies 2 is darker, dark brown or grey, and Fluvial facies 2 contains well developed layers of fluvially reworked plant remains (e.g. wood, leaves, seeds) and organic layers with thicknesses of several centimetres up to several decimetres. Loamy beds, several centimetres thick, can be present. When located near the surface, steeply inclined strata (14°–28°) are visible in the GPR profiles (Figure 3 and 4A through D). Fluvial facies 3 consists of (peaty) sandy, clayey or silt loam, clay or clayey peat. The colour of Fluvial facies 3 is dark brown, grey, green or blue. Fluvial facies 3 is generally humic (OM content 2%–4%) to very humic (OM content 4%–8%). The fluvial facies can be structureless, or can contain layers of fluvially reworked plant remains, organic and loamy layers with thicknesses of several millimetres to several centimetres. The total thickness of Fluvial facies 3 ranges from several decimetres up to 2.5 m. Fluvial facies 3 can be found within or on top of Fluvial facies 2. Thin deposits of Fluvial facies 3 can also be present in Fluvial facies 1. Fluvial facies 3 is often found along the margins of the valley or at the upstream side of a concave bank. Overbank deposits sometimes overlie Fluvial facies 3. The unit strongly reflects the GPR signal in contrast to Fluvial facies 1 and 2, and can consequently be recognized from the GPR profiles.

Different types of channel deposits can be interpreted from the described fluvial facies. Fluvial facies 1 was interpreted as point-bar deposits with a fining upward sequence. The GPR profile clearly shows lateral accretion surfaces, with a slope of approximately 1°–3°. Gently inclined strata

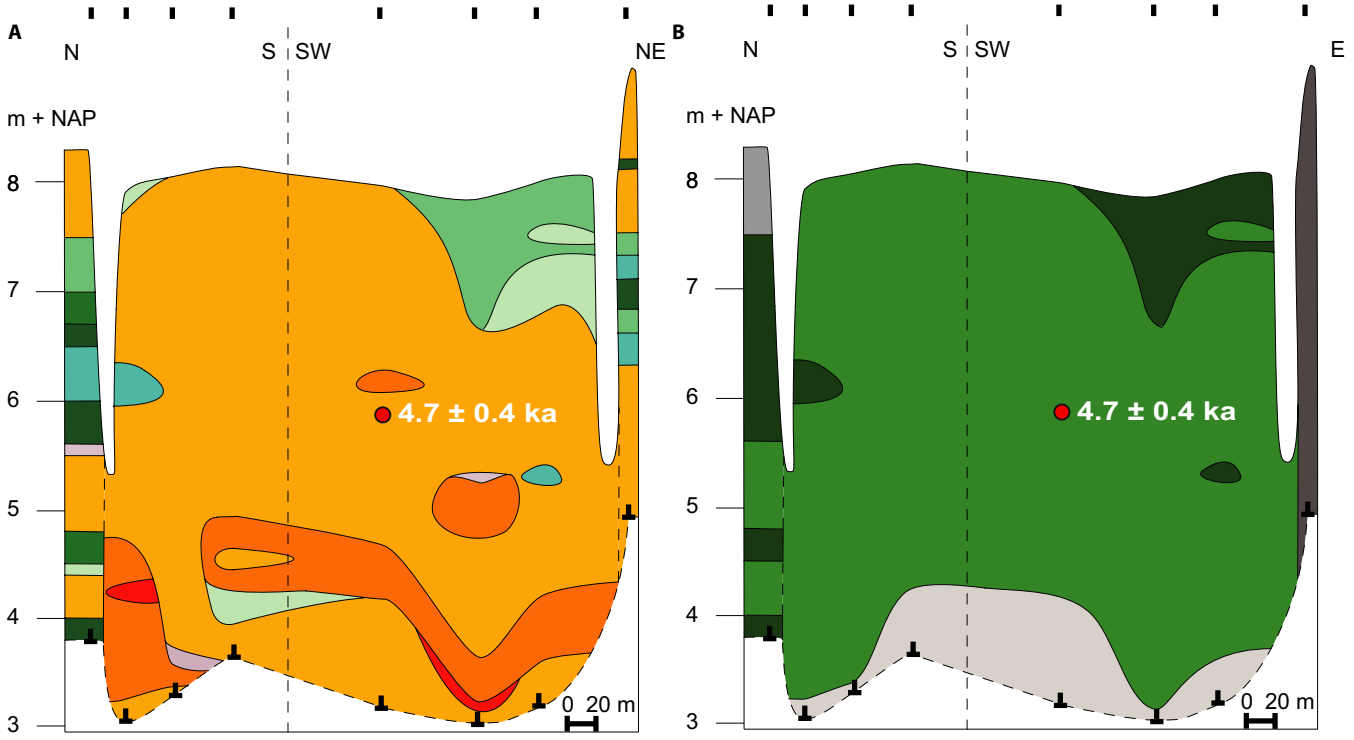

FIGURE 10 Cross-sections of the valley-fill (location in Figure 3E) including the OSL sample locations. (A) Lithological cross-section. (B) Lithogenetic cross-section. Legend indicated in Figure 5

may indicate a former river channel with a relatively large width/depth ratio (Leeder, 1973; Willis, 1989).

Fluvial facies 2 was also interpreted as point-bar deposits, with a clear fining upward sequence. The bottom and middle of the point-bar consist of thick intervals of stacked plant remains and organics, interlayered within the sandy point-bar. The presence of these thick intervals of plant remains result from the preservation of pool-infills on the river bed, or from counter-rotating flows on the convex side of a sharp river bend (Nanson, 2010; Blanckaert, 2011; Blanckaert *et al.*, 2013). The steep inclination in the GPR profiles (14°–28°) indicates that the associated channel had a relatively low width/depth ratio (Leeder, 1973).

Fluvial facies 3 mainly represents counterpoint deposits and upper or middle point-bar deposits. Counterpoint deposits occur as thick deposits of structureless or layered fine sediments and organics along the margins of the valley or on the upstream side of concave bends, which suggests deposition from suspension (Carey, 1969; Hickin, 1979; Page and Nanson, 1982; Makaske and Weerts, 2005; Smith *et al.*, 2009, 2011). Counter-rotating flows, flow separation, on the concave side of a river bend, promote the growth of these counterpoint deposits, which interfinger with point-bar deposits (Hickin, 1986; Makaske and Weerts, 2005; Smith *et al.*, 2011). Flow separation mainly occurs in sharp river bends (Nanson, 1980; 2010; Blanckaert, 2011; Blanckaert *et al.*, 2013). The interpretation given here matches the interpretations by Makaske and Weerts (2005) in the Hennisdijk channel-belt and Smith *et al.* (2011) in the meandering Peace River, who described the muddy, loamy and organic nature of these counterpoint deposits. Fluvial facies 3 can also be interpreted as middle or upper point-bar deposits, being part of the fining upward sequence of Fluvial facies 2. In this setting, Fluvial facies 3 was deposited near the downstream tail of a point-bar when flow separation occurs on the convex side of a sharp bend (Nanson, 1980; 2010; Blanckaert, 2011; Blanckaert *et al.*, 2013), explaining the relatively organic and fine-grained nature of point-bar deposits found in the Dommel River. Point-bars can consist of substantial quantities of organics, loam and mud, which seems especially characteristic of low-energy meandering river systems (Makaske, 1998 p. 225; Makaske and Weerts, 2005; Smith *et al.*, 2009).

3.2 | Cross-sections

The lithological and lithogenetic cross-sections are shown in Figures 5 through 10 and described below. The dating results are shown in Table 1, and also indicated in the cross sections. Figure 5 shows a cross-section of bend complexes A-1 and A-2 (Figure 3A). On the southern side, Fluvial facies 3 is interpreted as counterpoint deposits with a depth of *ca* 2 m, lying on top of Fluvial facies 2. These counterpoint deposits are relatively old (7.8 ± 0.8 ka), and hence the configuration relative to the palaeochannel, which is different from the recent Dommel River channel, cannot be

derived. Point-bar deposits on the inside of this bend complex are relatively young (0.6 ± 0.1 ka; Figure 5). Bend complex A-1 is bordered on the northern side by thick Holocene overbank deposits and in situ peat. The point-bar deposits of A-1 are older (2.3 ± 0.3 ka) than those of bend complex A-2.

Figure 6 shows a cross-section of bend complex B, where the current Dommel River lies along the valley side in the southern part. The valley side deposits (Figure 3C) consist of clay loam and very fine sands, overlying compacted in situ peat. Point-bar deposits (1.3 ± 0.3 ka) are located north of the current Dommel River, which reach channel-depth thickness (*ca* 4–4.5 m). The middle point-bar deposits consist of consolidated clayey and sandy peat (Fluvial facies 3). More point-bar deposits are located to the north, with peaty and loamy residual channel-fill sediments that reach as deep as the current Dommel River channel (Figure 6B). The in situ peat dates from 9.6 ± 0.2 ka. A narrow, relatively young point-bar deposit (*ca* 40 m wide, 0.7 ± 0.1 ka) is located north of the bend complex, with a similar depth as the residual channel-fill deposits. The GPR cross-section shows steeply inclined strata reflecting the lateral accretion surfaces of the point-bar, and horizontal layering north of the point-bar (Figure 4C,D). Fluvial facies 3 was interpreted here as counterpoint deposits (8.5 ± 1.2 ka), which seem to interfinger with point-bar deposits towards the north, and have a similar depth as the point-bar and residual channel deposits that are present in the cross-section.

Figure 7 shows a cross-section perpendicular to the cross-section in Figure 6. A small point-bar deposit is located on the western side, reaching channel-depth thickness. Point-bar deposits are located to the east, showing gently inclined lateral accretion surfaces (Figure 4E,F). Point-bar deposits (2.2 ± 0.3 ka) lie in between the peaty/loamy residual channel-fill and the valley side, and are similar in thickness to the current Dommel River depth (*ca* 4–4.5 m). The middle of these point-bar deposits are relatively organic and loamy (Fluvial facies 3). The loamy top of the valley side deposits is interpreted as the 'Brabant loam' described by Schokker (2003) and dates from 14.6 ± 1.4 ka (Kasse *et al.*, 2016).

Figure 8 shows a coring from the outer bank of bend complex B (Figure 3C). Surrounding corings on this part of the bend complex showed a similar succession of Fluvial facies 3 overlying Fluvial facies 2. This part was interpreted as counterpoint deposits dating from 2.5 ± 0.2 ka, and shows a similar age as the point-bar deposits on the inside of the bend complex in Figure 5. Figure 3C shows the extent of the counterpoint deposits along the valley side (all green-coloured corings) and the configuration relative to the channel that formed these counterpoint deposits.

Figure 9 shows counterpoint deposits along the south-eastern valley side of bend complex C (Figure 3E), dating from 2.8 ± 0.2 ka and interfingering with point-bar deposits. These counterpoint deposits are younger than the inner point-bar deposits (4.7 ± 0.4 ka), hence the younger counterpoint deposits were formed as a result of inward migration of the channel when it started to erode its older point-bar deposits. Both deposits reach a similar depth as the current Dommel River.

Figure 10 shows a cross-section perpendicular to the cross-section in Figure 9. This cross-section shows that the channel is bordered by Fluvial facies 3 on the northern side, and by the valley side on the northeastern side, which are interpreted as counterpoint deposits. Relatively narrow and thick (*ca* 4–4.5 m) point-bar deposits are present on the inside of the bend complex, with some loamy layers present within the point-bar deposits.

3.3 | Spatial configuration

Erosion-resistant deposits are abundantly present in the valley side and floodplain of the Dommel River, on both sides of the bend complexes (Figure 11). These erosion-resistant floodplain deposits consist of silt loam, clay loam and peaty deposits, with many reaching channel-depth thickness (Figures 5 through 10), and are consolidated at 2–4 m below the surface, further enhancing their resistance to erosion. The sedimentology of these fine-grained erosion-resistant deposits indicates that they mainly consist of residual channel-fill deposits, middle point-bar deposits and counterpoint deposits.

Easily erodible, sandy point-bar deposits are mostly present on the inside of bends, while hardly present along the outside of the oxbow bend complexes (Figure 11). These deposits are dated between 0.6 ± 0.1 ka and 4.7 ± 0.4 ka (Table 1). In contrast, the erosion-resistant deposits are generally older and dated between 1.3 ± 0.3 ka and 9.6 ± 0.2 ka (Table 1), reflecting the higher preservation potential of the erosion-resistant deposits (Figures 5 through 11).

3.4 | Morphodynamics

Several lines of evidence indicate that little aggradation (max. 0.5 m) occurred in the Dommel Valley during the Holocene. (a) Overbank deposits are nearly absent in the Dommel Valley; the only occurrences are on top of Late Glacial or Early Holocene deposits (e.g. Figures 5 through 7). (b) The base of the Early Holocene residual channel-fill (see Figure 6) occurs at the same depth as the base of the Late Holocene point-bar deposits. (c) Middle Holocene channel lags are often located at the same depth as the current Dommel channel floor (*ca* 4–4.5 m). (d) Lateral

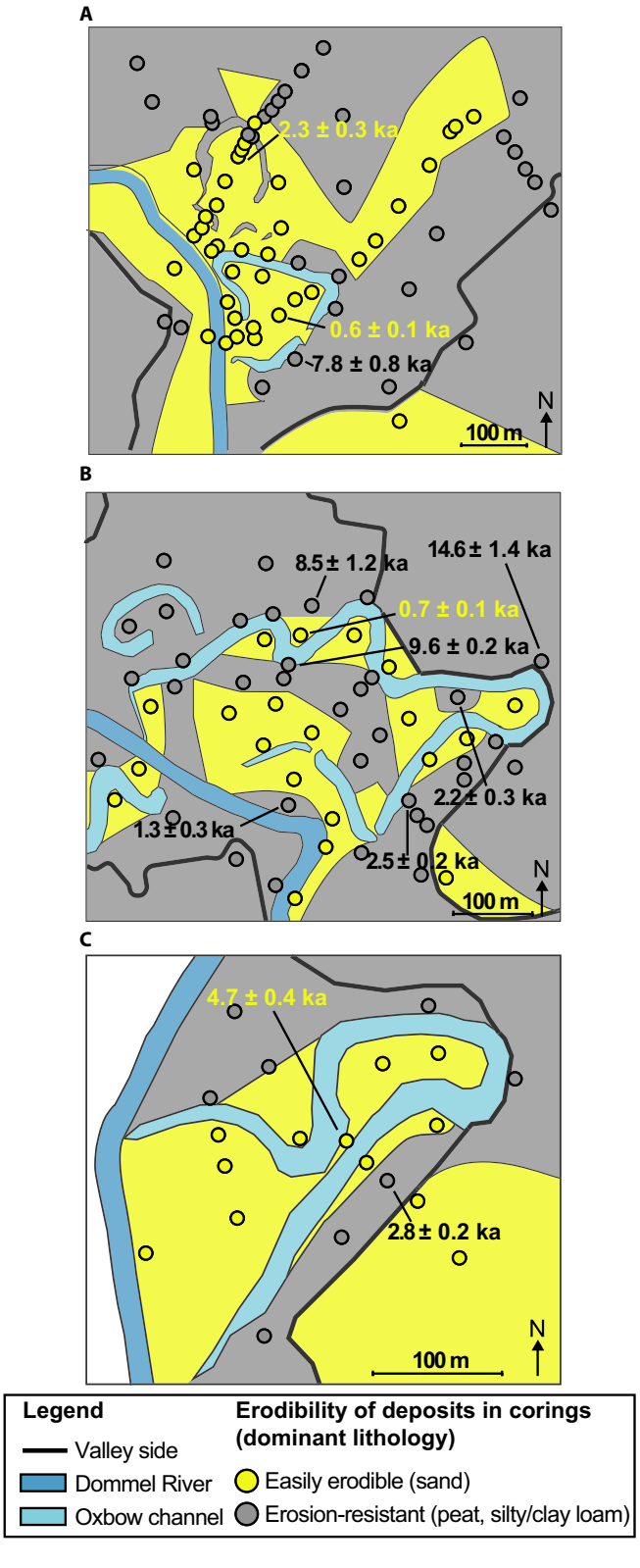

FIGURE 11 Simplified lithological maps showing the coring and dating (OSL and ^{14}C) locations. Colours of the cores indicate the erodibility and dominant lithology at that location; map colours are based on spatial interpretation, based on coring information, surface morphology and GPR cross-sections. Ages shown in black are obtained on erosion-resistant material, while those in yellow are from easily erodible deposits

accretion surfaces from the old point-bars (both Fluvial facies 1 and 2) always start within 0.5 m of the surface (e.g. Figure 4).

The configuration and age of channel deposits indicate that the Dommel River channel was largely constrained by its self-formed erosion-resistant deposits (Figure 11), and bends only migrated locally over relatively short distances where they were not restricted by erosion-resistant deposits in their outer banks. The Dommel River also shows relatively recent deposits of both easily erodible and erosion-resistant deposits (e.g. Figure 11C), but shows preferential erosion of the sandy deposits compared to the cohesive and organic deposits. Sharp secondary bends have formed within the primary bend complex forming a 'zig-zagging' channel planform lying in between the erosion-resistant deposits (Figure 11), resulting in a tortuous river planform with limited channel mobility. The reference here is to secondary bends when smaller bends form within a larger, primary bend. Sharp secondary river bends formed because the river eroded its own sandy point-bar deposits due to their lower resistance to erosion compared to the fine-grained depositional units outside of the primary bend complex. Hence, the hypothesis (Section 1) can be confirmed. In Section 4, the conceptual model of this self-constraining of low-energy meandering rivers will further be developed and tested for other meandering rivers.

4 | CONCEPTUAL MODEL

4.1 | Concepts of self-constraining low-energy meandering rivers

The self-constraining process of low-energy meandering rivers as conceptualized from the Dommel River reconstructions, is illustrated in Figure 12A. The relationship between the floodplain sediment composition, tortuosity and channel mobility and how they develop over time are elaborated on in Figure 12B through D.

The river mainly erodes its sandy point-bar deposits due to their lower resistance to erosion compared to other, more cohesive depositional units (Figure 12A). As a consequence of preservation differences, the fraction of easily erodible, non-cohesive sediments in the floodplain decreases over time (Figure 12B) (Smith *et al.*, 2009). Here, a self-constraining river is defined as 'a river of which the channel mobility is increasingly hampered over time by self-formed erosion-resistant banks'. This self-constraining is accompanied by increase in planform tortuosity due to the formation of sharp river bends (Figure 12A,C), which is a phenomenon commonly found in low-energy meandering rivers that are laterally restricted by erosion-resistant deposits (Turnbull *et al.*, 1966; Leeder and Bridges, 1975; Hickin, 1986;

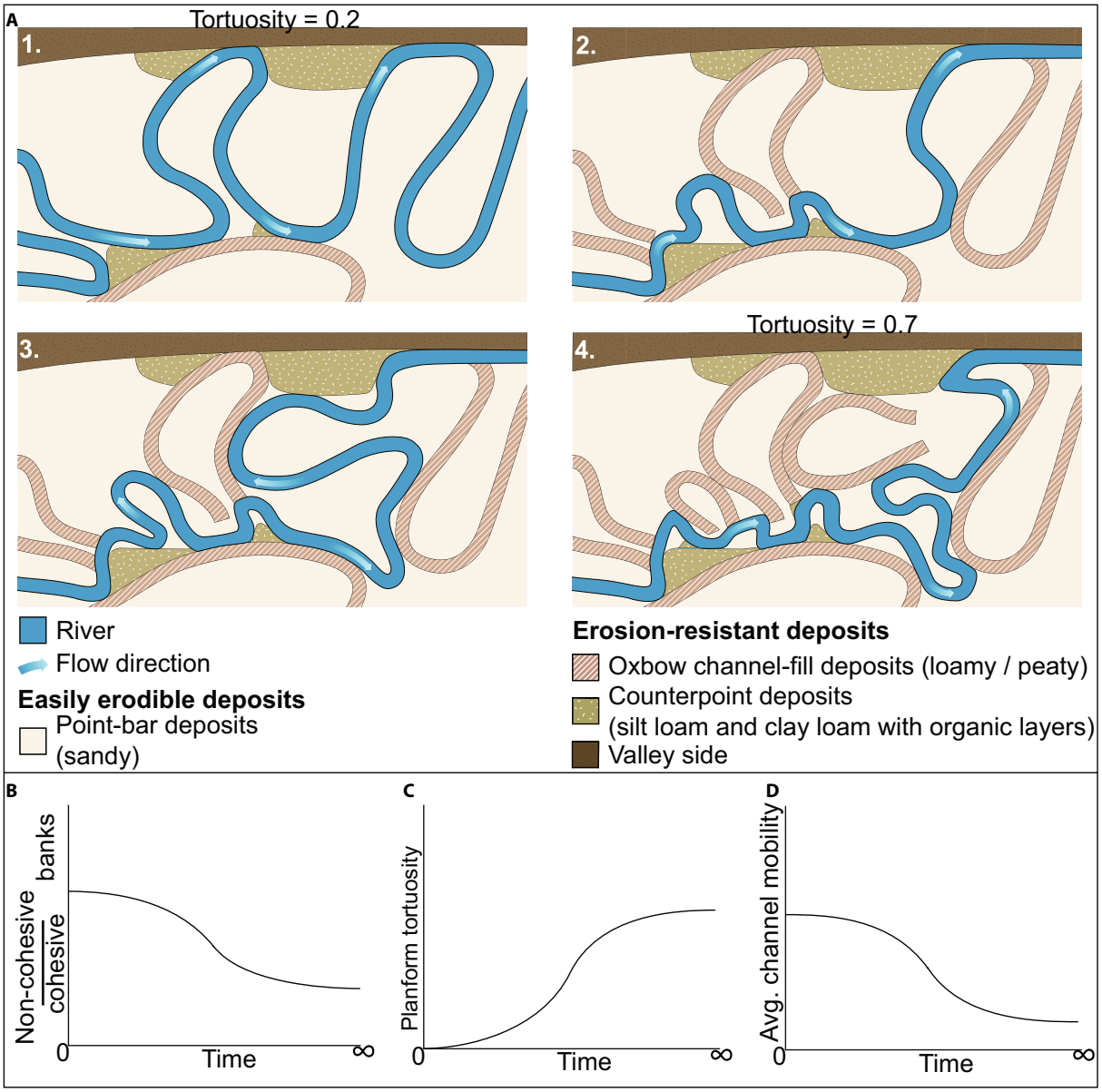

FIGURE 12 Self-constraining of a meandering river illustrated. (A) Conceptual maps showing the potential development of floodplain deposits and channel planform of a self-constraining river, assuming that neck cut-offs and counterpoint deposits immediately form erosion-resistant layers at the moment of cut-off or deposition. The tortuosity is indicated for the first and last timeframe. Conceptual graphs showing the long-term evolution of (B) bank cohesiveness, (C) planform tortuosity, and (D) average channel mobility

Güneralp and Rhoads, 2011). Flow separation in sharp river bends may lead to the formation of counterpoint deposits (Leeder and Bridges, 1975; Smith *et al.*, 2009; Figure 12A), which are generally cohesive due to incorporation of silt and organic material. Also cohesive middle point-bar deposits may form due to flow separation (Makaske and Weerts, 2005). Residual channel-fill deposits result from neck cut-offs that are promoted by preferential erosion of the sandy point bars instead of erosion of the fine-grained deposits (example of almost cut-off channel complex C, Figure 11C; Hooke, 2007). Residual channel-fills become fine-grained and organic when diversion angles to the cut-off channel are high (Constantine *et al.*, 2010), which is especially common in rivers with tortuous planforms. Newly formed fine-grained counterpoint deposits and residual channel-fills consist of erosion-resistant deposits that reach channel-depth thickness. Thus their thickness scales with river size, and they further foster the planform tortuosity and formation of sharp bends (Figure 12B,C). The erosion-resistance of these deposits increases even further with time as a result of consolidation.

Figure 12 shows the conceptual development of a self-constraining system over time, with a decrease in the ratio of non-cohesive/cohesive banks (Figure 12B), an increase in tortuosity (Figure 12C), and a decrease in channel mobility (Figure 12D). Quantifying these properties is not

possible with this dataset, but could be investigated using modelling experiments. Based on the conceptual model presented here, an initially exponentially increasing response is suggested due to the positive feedback between the formation of erosion-resistant deposits and increase in planform tortuosity. The average channel activity (Figure 12D) decreases simultaneously with the relative increase of erosion-resistant deposits in the vicinity of the channel (Figure 12B), slowing down the positive feedback loop, and eventually resulting in a low-energy meandering river with inhibited channel mobility (Figure 12D), predominantly cohesive banks (Figure 12B) and a tortuous planform (Figure 12C).

For simplicity, only the three main erosion-resistant deposits found in the Dommel River are shown in Figure 12A: residual channel-fill deposits, counterpoint deposits and the valley side. Other erosion-resistant deposits may be more dominant in other low-energy river systems, such as overbank deposits, fine-grained middle point-bar deposits or oblique accretion deposits (Page *et al.*, 2003; Słowik *et al.*, 2020), but they have the same effect on the river planform. Easily erodible deposits mainly consist of point-bar deposits for the Dommel River.

Sylvester *et al.* (2019) showed that bends with the highest curvatures show the highest migration rates. This was confirmed by observations on the intertidal mudflat, where the highest migration rates occurred in the sharp river bends due to flow separation, but the average river channel migration was low (Kleinhans *et al.*, 2009). Sharp bends show the highest displacement, because the remaining part of the river channel is relatively laterally stable due to the self-constraining. However, when comparing channel mobility between meandering rivers, the average channel mobility of rivers with sharp bends is expected to be generally lower than rivers with gentle, freely meandering bends (Hooke, 1980; 2007; Hudson and Kesel, 2000; Smith *et al.*, 2009; Bogoni *et al.*, 2017), because the channel mobility of self-constraining rivers is inhibited and limited to small sections of the floodplain (Figures 11 and 12).

4.2 | Applicability to other low-energy meandering rivers

To investigate whether the concepts of self-constraining are generally applicable, the information on potential specific stream power, erosion-resistance of the river banks and planform tortuosity were combined for the 47 different-sized meandering river reaches sampled for these data (Figure 13). As described in Section 2.6 these are all alluvial rivers with no evidence of strong modification by humans, all rivers are laterally connected with their floodplain, and are not strongly incising or aggrading (Kleinhans and Van den Berg, 2011).

The data shown in Figure 13 depict that rivers with tortuous planforms occur only when river energy is below the threshold required to erode the erosion-resistant banks (Julian and Torres, 2006). The minimum required potential specific stream power for bank erosion was derived by applying relationships from Julian and Torres (2006) and Kleinhans and Van den Berg (2011) (Equations 2 and 3):

$$\tau_c = 0.1 + 0.18\mathrm{SC} + 0.0028\mathrm{SC}^2 - 2.34\times10^{-5}\times\mathrm{SC}^3 \quad (2)$$

$$\omega_{\mathrm{crit}} = \frac{\tau_c^{1.5} C}{\sqrt{\rho g}} \quad (3)$$

where τ_c is the critical shear stress (Pa) to erode the SC-fraction (%) in the banks, and C is the Chézy coefficient ($m^{0.5}\ s^{-1}$), which was taken here as the median of the values for the rivers used in this analysis (36 $m^{0.5}\ s^{-1}$). Rivers below the threshold will predominantly erode easily erodible banks (with below average SC-fractions), resulting in an increasing fraction of erosion-resistant deposits over time. For river energy above the threshold the river is able to erode the erosion-resistant banks, resulting in a reduction of these erosion-resistant deposits (decreasing average SC-fractions) and a lower planform tortuosity (Figure 13). Gravel-bed rivers hardly develop tortuous planforms, because they require high river energy to mobilize the river bed material. At such energy levels they are able to erode banks irrespective of bank erodibility (Figure 13).

5 | DISCUSSION

5.1 | Prerequisites

Meandering rivers may become self-constraining under specific, but common, conditions. First, river energy should be insufficient to erode the cohesive depositional units, but sufficient to erode the non-cohesive material. These conditions apply to low-energy meandering rivers, especially sand-bed rivers that have a low threshold for sediment motion (*ca* 10^{-2} W/m^2 for sand-bed rivers). This analysis demonstrates that self-constraining occurs irrespective of river size (ranging from bankfull discharges of 22 m^3/s for the Dommel River to 1.7×10^4 m^3/s for the Purus River), provided that river energy is low (Figure 13). River energy is controlled by allogenic factors like climate and land cover that change over time (Candel *et al.*, 2018), and is therefore an allogenic control determining the occurrence of the autogenic processes of self-constraining.

Second, the river should transport a heterogeneous load of cohesive and non-cohesive material to be able to build a heterogeneous floodplain. Low-energy rivers commonly have a relatively fine-grained sediment load, and form floodplains with

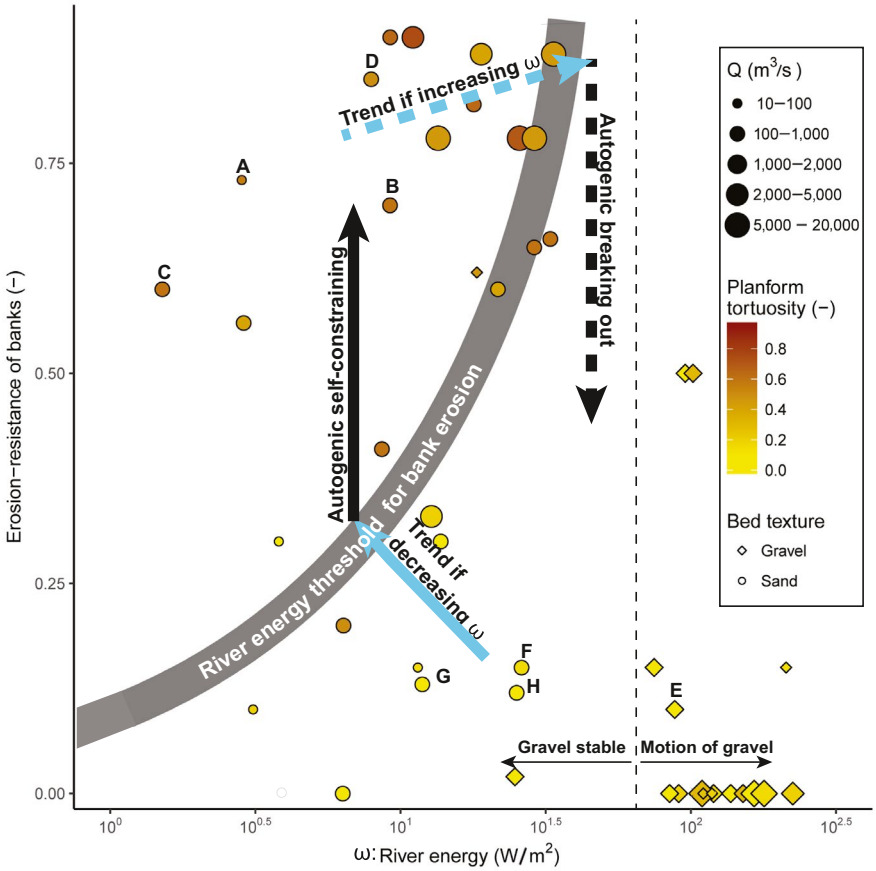

FIGURE 13 Erosion-resistance of banks (proxy: average silt-plus-clay fraction of river banks) plotted against river energy (proxy: potential specific stream power, ω) for a dataset of 47 rivers (Van den Berg, 1995; Kleinhans and Van den Berg, 2011). For each of the data points, effective channel-forming discharge (Q) (Kleinhans and Van den Berg, 2011), planform tortuosity and bed texture are shown. The thick grey line represents the minimum river energy needed to erode the river banks (Woodyer *et al.*, 1979; Page *et al.*, 2003; Julian and Torres, 2006; Kleinhans and Van den Berg, 2011). The thick arrows indicate the hysteresis cycle of self-constraining and breaking out, in black and blue the autogenic and allogenic processes, respectively. Dashed arrows represent hypothetical arrows. The labelled rivers correspond to rivers shown in Figure 1, or reconstructed Late-Glacial (LG) systems (see methods section on reconstruction). A through D refer to rivers with sharp bends, E through H refer to rivers with classical meandering planforms: A) Dommel River (Figure 1A), (B) Murrumbidgee River (Figure 1B), (C) Barwon River (Figure 1C), (D) San Antonio River (Figure 1D), (E) Waterton River (Figure 1E), (F) Assiniboine River (Figure 1F), (G) Late-Glacial Dommel River, (H) Late-Glacial Niers River

cohesive depositional units (Nanson and Croke, 1992). Rivers with a strictly non-cohesive sediment load will not develop self-formed erosion-resistant banks (Van Dijk *et al.*, 2012). Channel mobility of these rivers may only become restricted by, for example, vegetation (Van Oorschot *et al.*, 2016), soil formation (Bätz *et al.*, 2015), bank protection measures (Hesselink *et al.*, 2003) or peat formation (Candel *et al.*, 2017).

Finally, sufficient time is required during which the conditions fostering self-constraining of the channel prevail; thus channel belts should not frequently be abandoned due to avulsions. Such favourable conditions occur where rivers are located in a valley setting, in which valley sides may contribute to the self-constraining process when they are erosion-resistant (Figure 12A). Strong aggradation or incision may also reset the self-constraining, because they may potentially lead to overtopping or undercutting of the erosion-resistant deposits, respectively. Therefore, aggradation and incision rates should be relatively limited, as is the case with rivers used in this dataset (Kleinhans and Van den Berg, 2011).

5.2 | Implications

Although counter-intuitive, increase of river energy (e.g. because of climate or land cover changes) in self-constraining, low-energy meandering rivers may initially accelerate the self-constraining process and will lead to an increase in erosion-resistant deposits, provided that river energy is still below the threshold (Figure 13). If river energy exceeds the threshold, the self-constraining feedback loop is broken. It is conjectured that such rivers may then be able to erode the erosion-resistant deposits and partly replace them with easily erodible,

non-cohesive deposits (although convincing evidence of rivers that have crossed this threshold is presently lacking). The existence of two system states would create a hysteresis cycle (Figure 13).

A striking example of the self-constraining part of this hysteresis cycle is provided by river responses in many temperate regions during interglacial-glacial cycles. Many rivers in these regions were braiding during the Pleniglacial and changed to meandering during the Late Glacial (Vandenberghe, 1995; 2001). Valley slopes, bankfull discharges and thus river energy were high during the Late Glacial compared to the Holocene, due to low sea levels and high runoff from snowmelt peaks, and rivers formed their valleys within the non-cohesive river deposits that had previously been deposited by braided rivers (Mol *et al.*, 2000). Late-Glacial rivers were commonly high-energy, laterally migrating and planform tortuosity was low (Figure 13, e.g. the Late-Glacial Dommel and Niers Rivers; Kasse *et al.*, 2005). During the Holocene, river energy decreased, and this period provided sufficient time for rivers to develop tortuous planforms by self-constraining (Figures 12 and 13). Figure 13 indicates that these self-constraining meandering rivers can only break out of their constraints when river energy significantly increases to levels above the threshold. This may occur in a transition to a glacial period (Vandenberghe, 1995; 2008), although in such cases strong incision or aggradation may take place as well (violating the conditions discussed in this paper).

The hysteresis loop indicates that self-constraining, low-energy meandering rivers are highly resilient for bank erosion due to changes in river energy. This resilience may aid river management and reduce risk of infrastructure damage by channel migration, but there is always a risk of sudden unexpected and unwanted enhanced river dynamics when the threshold is crossed. Changes in the catchment land cover such as urbanization, peat extraction or deforestation may result in increased river energy by increasing peak flows (Candel *et al.*, 2018). When the increase in river energy is sufficient, the self-constraining rivers will be replaced by actively migrating meandering rivers. Such a response in river dynamics to an increase in energy may be unexpected, and may have catastrophic consequences. A channel pattern change was recently documented for the Overijsselse Vecht River (Candel *et al.*, 2018), showing that an increase in peak discharge changed a laterally stable river into a meandering river with lateral migration rates of 2–3 m/yr about 400 years ago.

6 | CONCLUSIONS

Based on a palaeogeographic reconstruction of the Dommel River (The Netherlands) it is shown here that low-energy meandering rivers may self-constrain their planform by preferential preservation of erosion-resistant deposits. This process explains the typical tortuous planform and low dynamics of low-energy rivers. The conceptual model of self-constraining is validated for a dataset of 47 meandering rivers, and from this analysis the critical threshold of river energy for self-constraining is derived. Reaches with a river energy below this critical threshold tend to have tortuous planforms and banks with a high silt-plus-clay fraction, in contrast to reaches with a river energy above this critical threshold. It is conjectured that a hysteresis cycle exists, which is controlled by the discharge regime, forced by allogenic factors such as land use and climate. Rivers self-constrain when their river energy is below the critical threshold for eroding cohesive banks, causing bank stability to increase over time, resulting in reduced channel mobility. Rivers break out of the self-constraining once the river energy crosses the critical threshold for eroding cohesive banks.

ACKNOWLEDGEMENTS

This research is part of the research programme RiverCare, supported by the Netherlands Organization for Scientific Research (NWO) and the Dutch Foundation of Applied Water Research (STOWA), and is partly funded by the Ministry of Economic Affairs under grant number P12-14 (Perspective Programme). M.G. Kleinhans was also supported by NWO (grant Vici 016.140.316/13710). This manuscript has benefited greatly from reviews by one anonymous reviewer and the associate editor. We would like to thank Alice Versendaal and Erna Voskuilen for their help with the OSL laboratory analysis, Meike Schipper for the illustration design of Figure 12, Renathe Kamstra for her help in the field, Martin Gibling, Jelmer Nijp and Elizabeth Chamberlain for discussion on the concepts. We would also like to thank Staatsbosbeheer, Brabants Landschap and water board De Dommel for the access to and the insight knowledge of the field sites.

CONFLICT OF INTEREST

The authors declare that they have no conflict of interest.

DATA AVAILABILITY

All data generated or analysed during this study are included in this published article and its supplementary information files, or are available in the DataverseNL repository; https://hdl.handle.net/10411/WO3KV0

ORCID

Jasper H. J. Candel https://orcid.org/0000-0001-8365-8673
Joep E. A. Storms https://orcid.org/0000-0002-8902-8493

REFERENCES

Aitken, M.J. (1998) *Introduction to Optical Dating: The Dating of Quaternary Sediments by the Use of photon-Stimulated Luminescence*. Oxford, UK: Oxford Univ. Press. 267 pages.

Bätz, N., Verrecchia, E.P. and Lane, S.N. (2015) The role of soil in vegetated gravelly river braid plains: more than just a passive response? *Earth Surface Processes and Landforms*, *40*, 143–156.

Berendsen, H.J. and Stouthamer, E. (2000) Late Weichselian and Holocene palaeogeography of the Rhine-Meuse delta, The Netherlands. *Palaeogeography, Palaeoclimatology, Palaeoecology*, *161*, 311–335.

Berendsen, H.J. and Stouthamer, E. (2001) Palaeogeographic development of the Rhine-Meuse delta, the Netherlands, Koninklijke van Gorcum. Assen. 268 Pages.

Bisschops, J.H. (1973) *Toelichtingen bijde geologische kaart van Nederland 1:50 000*. Haarlem: Rijks GeologischeDienst. 132 pages.

Blanckaert, K.C.F. (2011) Hydrodynamic processes in sharp meander bends and their morphological implications. *Journal of Geophysical Research: Earth Surface*, *116*, F0100322. https://doi.org/10.1029/2010jf001806

Blanckaert, K., Kleinhans, M.G., McLelland, S.J., Uijttewaal, W.S., Murphy, B.J., Kruijs, A. *et al*. (2013) Flow separation at the inner (convex) and outer (concave) banks of constant-width and widening open-channel bends. *Earth Surface Processes and Landforms*, *38*, 696–716.

Bogoni, M., Putti, M. and Lanzoni, S. (2017) Modeling meander morphodynamics over self-formed heterogeneous floodplains. *Water Resources Research*, *53*, 5137–5157.

Bøtter-Jensen, L., Andersen, C., Duller, G. and Murray, A. (2003) Developments in radiation, stimulation and observation facilities in luminescence measurements. *Radiation Measurements*, *37*, 535–541.

Bronk Ramsey, C. (2009) OxCal Program v4. 2. http://www.rlaha.ox.ac.uk/orau/oxcal.html

Camporeale, C., Perona, P., Porporato, A. and Ridolfi, L. (2005) On the long-term behavior of meandering rivers. *Water Resources Research*, *41*, W1240313.

Camporeale, C., Perona, P., Porporato, A. and Ridolfi, L. (2007) Hierarchy of models for meandering rivers and related morphodynamic processes. *Reviews of Geophysics*, *45*, RG100127.

Candel, J.H.J., Makaske, B., Storms, J.E.A. and Wallinga, J. (2017) Oblique aggradation: a novel explanation for sinuosity of low-energy streams in peat-filled valley systems. *Earth Surface Processes and Landforms*, *42*, 2679–2696. https://doi.org/10.1002/esp.4100

Candel, J.H.J., Kleinhans, M.G., Makaske, B., Hoek, W.Z., Quik, C. and Wallinga, J. (2018) Late Holocene channel pattern change from laterally stable to meandering – a palaeohydrological reconstruction. *Earth Surface Dynamics*, *6*, 723–741. https://doi.org/10.5194/esurf-6-723-2018

Carey, W.C. (1969) Formation of flood plain lands. *Journal of the Hydraulics Division*, *95*, 981–994.

Carlston, C.W. (1965) The relation of free meander geometry to stream discharge and its geomorphic implications. *American Journal of Science*, *263*, 864–885.

Constantine, J.A., Dunne, T., Piégay, H. and Mathias Kondolf, G. (2010) Controls on the alluviation of oxbow lakes by bed-material load along the Sacramento River, California. *Sedimentology*, *57*, 389–407.

Crosato, A. (2009) Physical explanations of variations in river meander migration rates from model comparison. *Earth Surface Processes and Landforms*, *34*, 2078–2086.

Cunningham, A.C. and Wallinga, J. (2010) Selection of integration time intervals for quartz OSL decay curves. *Quaternary Geochronology*, *5*, 657–666.

Cunningham, A.C. and Wallinga, J. (2012) Realizing the potential of fluvial archives using robust OSL chronologies. *Quaternary Geochronology*, *12*, 98–106.

Cunningham, A., Wallinga, J. and Minderhoud, P. (2011) Expectations of scatter in equivalent-dose distributions when using multi-grain aliquots for OSL dating. *Geochronometria*, *38*, 424–431.

Ferguson, R.I., Parsons, D.R., Lane, S.N. and Hardy, R.J. (2003) Flow in meander bends with recirculation at the inner bank. *Water Resources Research*, *39*, 39.

Frascati, A. and Lanzoni, S. (2009) Morphodynamic regime and long-term evolution of meandering rivers. *Journal of Geophysical Research: Earth Surface*, *114*, F0200212.

Friedkin, J.F. (1945) Laboratory study of the meandering of alluvial rivers. U.S. Waterways Experiments Station, Vicksburg, Mississippi, p. 40.

Galbraith, R.F., Roberts, R.G., Laslett, G., Yoshida, H. and Olley, J.M. (1999) Optical dating of single and multiple grains of quartz from Jinmium rock shelter, northern Australia: Part I, experimental design and statistical models. *Archaeometry*, *41*, 339–364.

Gibling, M.R. and Davies, N.S. (2012) Palaeozoic landscapes shaped by plant evolution. *Nature Geoscience*, *5*, 99–105.

Guérin, G., Mercier, N. and Adamiec, G. (2011) Dose-rate conversion factors: update. *Ancient TL*, *29*, 5–8.

Güneralp, İ. and Rhoads, B.L. (2011) Influence of floodplain erosional heterogeneity on planform complexity of meandering rivers. *Geophysical Research Letters*, *38*, L14401.

Hesselink, A.W., Weerts, H.J. and Berendsen, H.J. (2003) Alluvial architecture of the human-influenced river Rhine, The Netherlands. *Sedimentary Geology*, *161*, 229–248.

Hickin, E.J. (1979) Concave-bank benches on the Squamish River, British Columbia, Canada. *Canadian Journal of Earth Sciences*, *16*, 200–203.

Hickin, E.J. (1986) Concave-bank benches in the floodplains of Muskwa and Fort Nelson Rivers, British Columbia. *The Canadian Geographer/Le Géographe canadien*, *30*, 111–122.

Hickin, E.J. and Nanson, G.C. (1984) Lateral migration rates of river bends. *Journal of Hydraulic Engineering*, *110*, 1557–1567.

Hjulstrom, F. (1935) Studies of the morphological activity of rivers as illustrated by the river fyris, bulletin. *Geological Institute Upsalsa*, *25*, 221–527.

Hooke, J.M. (1980) Magnitude and distribution of rates of river bank erosion. *Earth Surface Processes and Landforms*, *5*, 143–157.

Hooke, J. (2007) Spatial variability, mechanisms and propagation of change in an active meandering river. *Geomorphology*, *84*, 277–296.

Hudson, P.F. and Kesel, R.H. (2000) Channel migration and meander-bend curvature in the lower Mississippi River prior to major human modification. *Geology*, *28*, 531–534.

Huisink, M. (2000) Changing river styles in response to Weichselian climate changes in the Vecht valley, eastern Netherlands. *Sedimentary Geology*, *133*, 115–134. https://doi.org/10.1016/S0037-0738(00)00030-0

Ikeda, S. and Parker, G. (1989) River meandering: Water Resources Monograph v. 12. American Geophysical Union, 485 p.

Janssen, C.R. (1972) The Palaeoecology of Plant Communities in the Dommel Valley, North Brabant, Netherlands. *Journal of Ecology*, *60*, 411–437. https://doi.org/10.2307/2258354

Julian, J.P. and Torres, R. (2006) Hydraulic erosion of cohesive riverbanks. *Geomorphology*, *76*, 193–206.

Kasse, C., Hoek, W.Z., Bohncke, S.J.P., Konert, M., Weijers, J.W.H., Cassee, M.L. *et al*. (2005) Late Glacial fluvial response of the

Niers-Rhine (western Germany) to climate and vegetation change. *Journal of Quaternary Science*, *20*, 377–394. https://doi.org/10.1002/jqs.923

Kasse, C., Van Balen, R., Bohncke, S., Wallinga, J. and Vreugdenhil, M. (2016) Climate and base-level controlled fluvial system change and incision during the last glacial–interglacial transition, Roer river, The Netherlands–western Germany. *Netherlands Journal of Geosciences*, *96*, 71–92.

Kleinhans, M.G. (2010) Sorting out river channel patterns. *Progress in Physical Geography*, *34*, 287–326.

Kleinhans, M.G. and Van den Berg, J.H. (2011) River channel and bar patterns explained and predicted by an empirical and a physics-based method. *Earth Surface Processes and Landforms*, *36*, 721–738.

Kleinhans, M.G., Schuurman, F., Bakx, W. and Markies, H. (2009) Meandering channel dynamics in highly cohesive sediment on an intertidal mud flat in the Westerschelde estuary, the Netherlands. *Geomorphology*, *105*, 261–276.

Lazarus, E.D. and Constantine, J.A. (2013) Generic theory for channel sinuosity. *Proceedings of the National Academy of Sciences*, *110*, 8447–8452.

Leeder, M. (1973) Fluviatile fining-upwards cycles and the magnitude of palaeochannels. *Geological Magazine*, *110*, 265–276.

Leeder, M. and Bridges, P. (1975) Flow separation in meander bends. *Nature*, *253*, 338–339.

Leopold, L.B. and Wolman, M.G. (1957) River channel patterns: braided, meandering, and straight. USGS Professional Paper, pp. 39–86.

Makaske, B. (1998) Anastomosing rivers: forms, processes and sediments. *Koninklijk Nederlands Aardrijkskundig Genootschap*, *249*, 1–298.

Makaske, B. and Weerts, H.J. (2005) Muddy lateral accretion and low stream power in a sub-recent confined channel belt, Rhine-Meuse delta, central Netherlands. *Sedimentology*, *52*, 651–668.

Mejdahl, V. (1979) Thermoluminescence dating: beta-dose attenuation in quartz grains. *Archaeometry*, *21*, 61–72.

Mol, J., Vandenberghe, J. and Kasse, C. (2000) River response to variations of periglacial climate in mid-latitude Europe. *Geomorphology*, *33*, 131–148. https://doi.org/10.1016/S0169-555X(99)00126-9

Motta, D., Abad, J.D., Langendoen, E.J. and Garcia, M.H. (2012a) The effects of floodplain soil heterogeneity on meander planform shape. *Water Resources Research*, *48*, W0951817.

Motta, D., Abad, J.D., Langendoen, E.J. and Garcia, M.H. (2012b) A simplified 2D model for meander migration with physically-based bank evolution. *Geomorphology*, *163*, 10–25.

Nanson, G.C. (1980) Point bar and floodplain formation of the meandering Beatton River, northeastern British Columbia, Canada. *Sedimentology*, *27*(1), 3–29.

Nanson, R.A. (2010) Flow fields in tightly curving meander bends of low width-depth ratio. *Earth Surface Processes and Landforms*, *35*, 119–135.

Nanson, G.C. and Croke, J.C. (1992) A genetic classification of floodplains. *Geomorphology*, *4*, 459–486. https://doi.org/10.1016/0169-555X(92)90039-Q

Neal, A. (2004) Ground-penetrating radar and its use in sedimentology: principles, problems and progress. *Earth-Science Reviews*, *66*, 261–330. https://doi.org/10.1016/j.earscirev.2004.01.004

Page, K. and Nanson, G. (1982) Concave-bank benches and associated floodplain formation. *Earth Surface Processes and Landforms*, *7*, 529–543.

Page, K., Nanson, G. and Frazier, P. (2003) Floodplain formation and sediment stratigraphy resulting from oblique accretion on the Murrumbidgee River, Australia. *Journal of Sedimentary Research*, *73*, 5–14.

Prescott, J.R. and Hutton, J.T. (1994) Cosmic ray contributions to dose rates for luminescence and ESR dating: large depths and long-term time variations. *Radiation Measurements*, *23*, 497–500.

Reimer, P.J., Bard, E., Bayliss, A., Beck, J.W., Blackwell, P.G., Bronk Ramsey, C. *et al*. (2013) IntCal13 and Marine13 radiocarbon age calibration curves 0–50,000 years cal BP. *Radiocarbon*, *51*, 1111–1150.

Schokker, J. (2003) *Patterns and processes in a Pleistocene fluvio-aeolian environment*. Utrecht: Utrecht University.

Schokker, J. and Koster, E.A. (2004) Sedimentology and facies distribution of Pleistocene cold-climate aeolian and fluvial deposits in the Roer Valley Graben (southeastern Netherlands). *Permafrost and Periglacial Processes*, *15*(1), 1–20.

Schumm, S.A. (1963) Sinuosity of alluvial rivers on the Great Plains. *Geological Society of America Bulletin*, *74*, 1089–1100.

Seminara, G. (2006) Meanders. *Journal of Fluid Mechanics*, *554*, 271–297.

Słowik, M., Dezső, J., Kovács, J. and Gałka, M. (2020) The formation of low-energy meanders in loess landscapes (Transdanubia, central Europe). *Global and Planetary Change*, *184*, 103071.

Smith, D.G., Hubbard, S.M., Leckie, D.A. and Fustic, M. (2009) Counter point bar deposits: lithofacies and reservoir significance in the meandering modern Peace River and ancient McMurray Formation, Alberta, Canada. *Sedimentology*, *56*, 1655–1669.

Smith, D.G., Hubbard, S.M., Lavigne, J.R., Leckie, D.A. and Fustic, M. (2011) Stratigraphy of counter-point-bar and eddy-accretion deposits in low-energy meander belts of the Peace-Athabasca Delta, northeast Alberta, Canada: From River to Rock Record: The Preservation of Fluvial Sediments and Their Subsequent Interpretation. *SEPM Special Publication*, *97*, 143–152.

Stølum, H.-H. (1996) River meandering as a self-organization process. *Science*, *271*, 1710–1713.

Struiksma, N., Olesen, K., Flokstra, C. and de Vriend, H. (1985) Bed deformation in curved alluvial channels. *Journal of Hydraulic Research*, *23*, 57–79.

Sylvester, Z., Covault, J.A. and Durkin, P. (2019) High curvatures drive river meandering. *Geology*, *47*(3), 263–266. https://doi.org/10.1130/g45608.1

TNO (2015) DINOLoket. https://www.dinoloket.nl/ondergrond modellen

Turnbull, W.J., Krinitzky, E.L. and Weaver, F.J. (1966) Bank erosion in soils of the lower Mississippi valley. *Journal of the Soil Mechanics and Foundations Division*, *92*, 121–136.

Van Alphen, J., Bloks, P. and Hoekstra, P. (1984) Flow and grainsize pattern in a sharply curved river bend. *Earth Surface Processes and Landforms*, *9*, 513–522.

Van de Meene, E., Van der Staay, J. and Teoh, L.H. (1979) *The Van der Staay suction-corer: a simple apparatus for drilling in sand below groundwater table*. Haarlem: Rijks Geologische Dienst.

Van den Berg, J.H. (1995) Prediction of alluvial channel pattern of perennial rivers. *Geomorphology*, *12*, 259–279.

Van der Hammen, T. (1971) The Upper Quaternary of the Dinkel Valley:(Twente, Eastern Overijssel, the Netherlands), Uitgevers-Maatschappij" Ernest van Aelst".

Van der Linden, J.A. (1973) *Topographische en Militaire kaart van het Koningrijk der Nederlanden*. Bussum: Fibula-Van Dischoeck, 75 p.

Van Dijk, W., Lageweg, W. and Kleinhans, M. (2012) Experimental meandering river with chute cutoffs. *Journal of Geophysical Research:*

Earth Surface. *117*(F3), F0302318. https://doi.org/10.1029/2011JF002314

Van Heteren, S., Fitzgerald, D.M., Mckinlay, P.A. and Buynevich, I.V. (1998) Radar facies of paraglacial barrier systems: coastal New England, USA. *Sedimentology*, *45*(1), 181–200.

Van Leeuwaarden, W. (1982) *Palynological and macropalaeobotanical studies in the development of the vegetation mosaic in Eastern Noord-Brabant (in the Netherlands) during Lateglacial and early Holocene times*. Utrecht: Leeuwaarden.

Van Oorschot, M., Kleinhans, M., Geerling, G. and Middelkoop, H. (2016) Distinct patterns of interaction between vegetation and morphodynamics. *Earth Surface Processes and Landforms*, *41*, 791–808.

Vandenberghe, J. (1995) Timescales, climate and river development. *Quaternary Science Reviews*, *14*, 631–638. https://doi.org/10.1016/0277-3791(95)00043-O

Vandenberghe, J. (2001) A typology of Pleistocene cold-based rivers. *Quaternary International*, *79*, 111–121. https://doi.org/10.1016/S1040-6182(00)00127-0

Vandenberghe, J. (2008) The fluvial cycle at cold–warm–cold transitions in lowland regions: A refinement of theory. *Geomorphology*, *98*, 275–284. https://doi.org/10.1016/j.geomorph.2006.12.030

Vandenberghe, J. and Bohncke, S. (1985) The Weichselian Late Glacial in a small lowland valley (Mark River, Belgium and The Netherlands)[Le Weichselien tardiglaciaire dans une vallée des plaines basses (La rivière Mark, Belgique et Pays-Bas)]: Bulletin de l'Association française pour l'Étude du. *Quaternaire*, *22*, 167–175.

Vandenberghe, J. and Van Huissteden, J. (1988) Fluvio-aeolian interaction in a region of continuous permafrost. Proceedings of the V International Conference on PermafrostTrondheim, Norway. pp. 876–881.

Vandenberghe, D., De Corte, F., Buylaert, J.-P. and Kučera, J. (2008) On the internal radioactivity in quartz. *Radiation Measurements*, *43*, 771–775.

Van Heerd, R. and Van't Zand, R. (1999) Productspecificatie Actueel Hoogtebestand Nederland. Rijkswaterstaat Meetkundige Dienst, Delft.

Vermeulen, B., Hoitink, A., Berkum, S. and Hidayat, H. (2014) Sharp bends associated with deep scours in a tropical river: The river Mahakam (East Kalimantan, Indonesia). *Journal of Geophysical Research: Earth Surface*, *119*, 1441–1454.

Vink, A.P.A. (1949) Bijdrage tot de kennis van loess en dekzanden: in het bijzonder van de zuidoostelijke Veluwe, Veenman.

Wallinga, J. and Van der Staay, J. (1999) Sampling in water logged sands with a simple hand operated corer. *Ancient TL*, *17*, 59–61.

Waterschap De Dommel (1941) Waterschap De Dommel, 1862–1941: Stukken betreffende de uitvoering van verbeteringswerken aan de rivier de Dommel, alsmede aan de kaden, duikers en kokers, Den Bosch, BHIC.

Willis, B.J. (1989) Palaeochannel reconstructions from point bar deposits: a three-dimensional perspective. *Sedimentology*, *36*, 757–766. https://doi.org/10.1111/j.1365-3091.1989.tb01744.x

Wintle, A.G. and Murray, A.S. (2006) A review of quartz optically stimulated luminescence characteristics and their relevance in single-aliquot regeneration dating protocols. *Radiation Measurements*, *41*, 369–391.

Woodyer, K., Taylor, G. and Crook, K. (1979) Depositional processes along a very low-gradient, suspended-load stream: the Barwon River, New South Wales. *Sedimentary Geology*, *22*, 97–120.

SUPPORTING INFORMATION

Additional supporting information may be found online in the Supporting Information section.

How to cite this article: Candel JHJ, Makaske B, Kijm N, Kleinhans MG, Storms JEA, Wallinga J. Self-constraining of low-energy rivers explains low channel mobility and tortuous planforms. *Depositional Rec*. 2020;6:648–669. https://doi.org/10.1002/dep2.112